ARTICLE IN PRESS

Nature Communications

https://doi.org/10.1038/s41467-026-71996-7

Article in Press

Histone methylation defines c-Jun/Sox2/Hif1α axis that controls stemness and tumor progression in squamous cell carcinoma

Received: 17 February 2025

Accepted: 6 April 2026

Cite this article as: Mehta, D., Paradkar, A., Rekhi, B. *et al.* Histone methylation defines c-Jun/Sox2/Hif1α axis that controls stemness and tumor progression in squamous cell carcinoma. *Nat Commun* (2026). https://doi.org/10.1038/s41467-026-71996-7

Darshan Mehta, Akshay Paradkar, Bharat Rekhi, Prakash Nayak, Bhabani Mohanty, Pradip Chaudhari, Poonam Gera, Swapnil Rane, Pankaj Chaturvedi & Sanjeev K. Waghmare

We are providing an unedited version of this manuscript to give early access to its findings. Before final publication, the manuscript will undergo further editing. Please note there may be errors present which affect the content, and all legal disclaimers apply.

If this paper is publishing under a Transparent Peer Review model then Peer Review reports will publish with the final article.

ARTICLE IN PRESS

© The Author(s) 2026. **Open Access** This article is licensed under a Creative Commons Attribution-NonCommercial-NoDerivatives 4.0 International License, which permits any non-commercial use, sharing, distribution and reproduction in any medium or format, as long as you give appropriate credit to the original author(s) and the source, provide a link to the Creative Commons licence, and indicate if you modified the licensed material. You do not have permission under this licence to share adapted material derived from this article or parts of it. The images or other third party material in this article are included in the article's Creative Commons licence, unless indicated otherwise in a credit line to the material. If material is not included in the article's Creative Commons licence and your intended use is not permitted by statutory regulation or exceeds the permitted use, you will need to obtain permission directly from the copyright holder. To view a copy of this licence, visit http://creativecommons.org/licenses/by-nc-nd/4.0/.

ARTICLE IN PRESS

Title: Histone methylation defines c-Jun/Sox2/Hif1α axis that controls stemness and tumor progression in squamous cell carcinoma

Darshan Mehta[1, 2], Akshay Paradkar[1, 2], Bharat Rekhi[3], Prakash Nayak[4], Bhabani Mohanty[5], Pradip Chaudhari[2,5], Poonam Gera[6], Swapnil Rane[2,7], Pankaj Chaturvedi[8], and Sanjeev K Waghmare[1, 2*]

1 Stem Cell Biology Group, Waghmare Lab, Cancer Research Institute, Advanced Centre for Treatment Research and Education in Cancer (ACTREC), Tata Memorial Centre, Kharghar, Navi Mumbai 410210, Maharashtra, India.

2 Homi Bhabha National Institute, Training School Complex, Anushakti Nagar, Mumbai 400085, India.

3 Department of Pathology, Tata Memorial Hospital, Homi Bhabha National Institute, Mumbai 400085, India.

4 Tata Memorial Hospital, Homi Bhabha National Institute, Mumbai, India

5 Small Animal Imaging Facility (SAIF), Advanced Centre for Treatment Research and Education in Cancer (ACTREC), Tata Memorial Centre, Kharghar, Navi Mumbai 410210, Maharashtra, India.

6 Cancer Research Institute, ACTREC, Tata Memorial Centre, Kharghar, Navi Mumbai, Maharashtra 410210, India

7 Department of Pathology, Advanced Centre for Treatment, Research and Education in Cancer, Tata Memorial Centre, Navi Mumbai, India

8 Tata Memorial Centre-Advanced Centre for Treatment Research and Education in Cancer ACTREC, Kharghar, Navi Mumbai, Maharashtra 410210, India

***Correspondence**: Sanjeev K Waghmare, Ph.D., Stem Cell Biology Group, Waghmare Lab, Cancer Research Institute, Advanced Centre for Treatment Research and Education in Cancer (ACTREC), Tata Memorial Centre, Kharghar, Navi Mumbai 410210, Maharashtra, India.

E-mail: swaghmare@actrec.gov.in **phone:** +91-22-2740-5122, Fax: +91-22-2740-5085

ARTICLE IN PRESS

ARTICLE IN PRESS

Abstract:

Squamous cell carcinomas (SCCs) originate from various sites that show poor survival due to the presence of cancer stem cells (CSCs), which impart therapy resistance. However, the crosstalk of molecular mechanisms regulating CSCs maintenance in skin and oral SCC is poorly understood. Here, we show that the whole-transcriptome profile of CSCs from skin SCC patients reveals upregulation in expression of genes associated with global hypermethylation, enhanced non-canonical Wnt signaling, and glycolysis, thereby activating the c-Jun/Sox2/Hif1α axis. Thus, it suggests crosstalk among epigenetics/signaling/metabolism in skin and oral SCCs. Importantly, the combination of Decitabine (DAC), a methyltransferase inhibitor, and a RAC1 non-canonical Wnt inhibitor (RAC1i) in skin and oral SCC xenograft mouse models reduces global hypermethylation and non-canonical Wnt signaling, thereby attenuating the c-Jun/Sox2/Hif1α axis, stemness, and tumorigenic potential. Overall, our findings show that the combination of DAC and RAC1i may improve the clinical outcomes in patients with skin and oral SCC.

ARTICLE IN PRESS

ARTICLE IN PRESS

1. Introduction:

Squamous cell carcinomas (SCCs) are common epithelial cancers that significantly contribute to global mortality. The subtypes of SCCs include skin SCC, oral SCC, and lung SCC, etc., each of which exhibits molecular changes and clinical behaviours. However, skin and oral SCCs showed the highest mortality rate worldwide due to metastasis either in the regional lymph nodes or distant organs. Recent reports have emphasized that the complex interaction between genetic mutations and epigenetic modification is important in the development and progression of SCCs[1]. Epigenetic modifications, such as DNA methylation and histone modifications, play pivotal roles in regulating gene expression. DNA methylation is the most common form, affecting gene expression by altering chromatin structure and recruiting modifiers like DNMT1, DNMT3a, and DNMT3b[2,3]. Furthermore, KMT2D, a histone methyltransferase, acts as a tumor suppressor in head and neck squamous cell carcinoma (HNSCC) and plays an important role in inhibiting of tumor progression. KMT2D mutation or deletion is involved in the development and aggressiveness of HNSCC[4]. Despite the crucial role of epigenetics in SCCs, elucidating the underlying molecular mechanism is essential. An important aspect of SCCs is the dysregulation of the Wnt signaling pathway (canonical/non-canonical Wnt signaling), which plays crucial roles in proliferation, differentiation, and migration that are associated with cancer stem cells (CSCs) maintenance, tumor aggressiveness, and resistance to therapy in SCC[5–9]. Multiple studies highlighted the aberrations of Wnt signaling in cancers such as HNSCC[5], breast cancer[6], glioblastoma[7], skin cancer[8], and liver cancer[10]. Furthermore, Wnt signaling is regulated by various antagonists, such as Wnt inhibitory protein-1 (WIF1), Dickkopf (DKK), and secretory frizzled proteins (SFRPs)[11]. SFRPs are majorly upregulated during early embryogenesis of mice[12]. Sfrp1 is involved in the regulation of hematopoietic stem cells (HSCs) through the canonical Wnt signaling pathway[13]. Our laboratory also showed that Sfrp1 regulates the hair follicle stem cell (HFSCs) pool through the BMP-AKT-GSK3B axis[14]. On the other hand, the loss of Sfrp1 in glioblastoma activates canonical Wnt signaling[15]. Moreover, low expression of Sfrp1 is associated with poor overall survival (OS) in glioblastoma patients[16]. Furthermore, miRNA-27a binds and targets Sfrp1, which subsequently activates Wnt/β-catenin signaling, resulting in cell proliferation of gastric and breast cancer[17,18]. Sfrp1 loss showed an increased tumor initiation and EMT in murine skin CSCs[19].

Recent studies have demonstrated the interaction between epigenetic modifiers and Wnt signaling, in which DNMT1 or EZH2 stabilizes β-catenin by recruiting the USP7 (deubiquitinase) in

ARTICLE IN PRESS

colorectal and neuronal cancer cells[20,21]. However, the role of epigenetic regulation in non-canonical Wnt signaling remains obscure in skin and oral SCC. Hence, investigating the crosstalk between non-canonical Wnt signaling and epigenetic modification would unravel an important molecular network that may contribute to the progression of skin and oral SCC. Moreover, SCCs undergo significant metabolic reprogramming; one of the important characteristics is increased glycolysis[22]. This high proliferative demand of tumor cells shifts the flux towards aerobic glycolysis and contributes to the heterogeneous metabolic landscape within the tumors[23,24]. It has been observed that α-ketoglutarate regulates the Wnt signaling in colon cancer[24]. Similarly, aberrant activation of the Wnt signaling pathway promotes aerobic glycolysis in colon cancer[25,26]. Wnt/β-catenin signaling through CEBPA/FOXA1 regulates amino acid metabolism by targeting histidine ammonia lyase (HAL) in liver cancer[27]. Furthermore, the overexpression of LRP5 increases Wnt/β-catenin signaling and thereby promotes aerobic glycolysis in gastric cancer[28]. However, the role of epigenetic modifiers in regulating non-canonical Wnt signaling, which influences metabolic reprogramming, remains elusive in skin and oral SCCs.

In this work, our whole transcriptome profile (RNA sequencing) of advanced-stage skin SCC patient samples shows enrichment for genes regulating histone and DNA methylation, EMT markers, non-canonical Wnt signaling, and glycolysis. We uncover that histone and DNA methylation of the *SFRP1* promoter enhances non-canonical Wnt signaling (*WNT7B, c-JUN*) in both skin and oral SCC. Importantly, we show that *c-JUN* regulates the SOX2 promoter, a key transcription factor that maintains tumour stemness. Furthermore, ChIP-qPCR data reveal that *SOX2* regulates *HIF1α*, which directly controls the expression of key glycolytic enzymes such as *HK2* and *LDHA* in skin and oral SCC. Importantly, we find that the combination of Decitabine (DAC) (DNA methylation inhibitor) and RAC1i (non-canonical Wnt signaling inhibitor) leads to a significant reduction in (~75-80%) tumor growth of skin and oral SCC. Our RNA sequencing, in combination of DAC and RAC1i, reveals a reduction in DNA methylation, which restores SFRP1 levels by decreasing non-canonical Wnt signaling, EMT markers, and glycolysis, thereby reducing cancer stemness and in vivo tumorigenic and metastatic potential in skin and oral SCC. Our study paves the way for the development of targeted therapies in skin and oral SCC.

ARTICLE IN PRESS

2. Results

➢ Loss of SFRP1 increases non-canonical Wnt signaling and glycolysis in advanced-stage human skin SCC and oral SCC patients

To delineate the molecular signaling in advanced-stage human skin SCC patients, we collected advanced-stage skin SCC patient samples (**n=6**) and normal skin (adjacent margin) (**n=6**). Furthermore, we performed FACS on advanced-stage skin SCC patient samples and normal skin (adjacent margin) to isolate CSCs using the CD133 marker (**Fig. 1a**). Our data showed that normal skin (adjacent margin) has CD133- cells (**99.99%**), which were considered non-CSCs. Subsequently, we collected CD133+ (CSCs) from patients with skin SCC (**~2-3%**) for RNA sequencing (**Fig. 1b**). Our RNA sequencing data revealed the loss of SFRP1 in the skin CSCs as compared to normal skin (adjacent margin) CD133- (non-CSCs), and enrichment in the genes involved in the non-canonical Wnt signaling, EMT markers, and glycolytic genes (**Supplementary Fig.1a-c**), suggesting a correlation among them.

Similarly, we have validated the human skin CSCs RNA sequencing data by Real-Time PCR, which revealed upregulation of non-canonical Wnt signaling (*WNT7B*), stemness marker (*SOX2)*, EMT markers (*VIMENTIN, TWIST1, ZEB1, ZEB2)*, and glycolytic genes (*SLC2a1, SLC2a2, HK2, LDHA, SIRT2*) in skin SCC patients CSCs as compared to normal skin (adjacent margin) (non-CSCs) (**Fig. 1c**). Furthermore, we have also checked the levels of non-canonical Wnt signaling in the skin SCC patients and normal skin (adjacent margin) by western blot analysis. Our data revealed a reduction in SFRP1 levels, while upregulation in levels of non-canonical Wnt signaling (WNT7B, DVL2, RAC1, JNK, c-FOS, c-JUN, SOX2) in skin SCC patients as compared to normal skin (adjacent margin) (**Supplementary Fig. 2a & b**).

In addition, epithelial tissues such as skin and oral epithelia share similarities in tissue structure and function, as well as in tumor progression and metastasis. We sought to understand whether a similar relationship exists between skin and oral SCC. Hence, we performed TCGA data analysis from UCSC Xena for human oral SCC primary tumor (**n=520**) and normal solid tissue (**n=43),** which showed an upregulation in expression of *EZH2, WNT7B,* and *c-JUN,* while downregulation in gene expression of *SFRP1* in oral SCC primary tumor as compared to the normal solid tissue (**Supplementary Fig. 3a-c**). Further, we have also performed the correlation analysis between OS and expression levels of *SFRP1, WNT7B*, and c-*JUN* genes from the publicly available TCGA of HNSCC database, which showed that low SFRP1 expression is associated with poor OS (**p=0.001**)

ARTICLE IN PRESS

in HNSCC patients (**Supplementary Fig. 3a-c**). Similarly, high c-JUN expression is associated with poor OS (**p=0.029**) in HNSCC patients. However, we did not find a significant association of EZH2 and WNT7B expression with OS in TCGA HNSCC database (**Supplementary Fig. 3a-c**).

Furthermore, to validate the observation of the TCGA database, we performed immunohistochemistry (IHC) of SFRP1, WNT7B, and c-JUN (non-canonical Wnt signaling) on skin SCC patient samples (**n=28**), normal skin samples (adjacent margin) (**n=10**), oral SCC patient samples (**n=59**), and normal oral mucosa samples (adjacent margin) (**n=12**). We observed low SFRP1 levels and increased levels of WNT7B and c-JUN in skin SCC patient samples as compared to the normal skin (adjacent margin), and oral SCC patient samples as compared to normal oral mucosa (adjacent margin) (**Fig. 1d-h)**. Quantitative comparison of the skin and oral SCC IHC scores showed significant upregulation of WNT7B levels **(~1.5-fold)** in skin SCC patients as compared to oral SCC patients. We have also observed a reduction in SFRP1 levels **(~3-4-fold**) in skin SCC patients as compared to oral SCC patients. However, we have not found the differences in the IHC scores of c-JUN between skin and oral SCC patients (**Supplementary Fig. 4a**).

Importantly, we observed significant negative correlations between SFRP1 and WNT7B, and c-JUN, in skin and oral SCC patients. (**Supplementary Fig. 5a & b)**. In addition, we observed that decreased levels of SFRP1 and increased levels of WNT7B, c-JUN are associated with poor OS by Kaplan-Meier plots in skin and oral SCC patients (**Supplementary Fig. 6a-f**).

Overall, our data showed that increased non-canonical Wnt signaling is associated with poor OS in skin and oral SCC patients.

ARTICLE IN PRESS

- **Skin cell line CSCs showed enhanced non-canonical Wnt signaling and glycolysis:**

To investigate the detailed molecular mechanisms in skin CSCs, we isolated CSCs and non-CSCs from the skin SCC cell lines A3886 and ACSCC1. We have also used primary human epidermal keratinocytes (HEKa) as a control.

Our result showed 9.13% population of skin CSCs (CD133+) in the A3886 cell line, while remaining cells were negative for CD133 (non-CSCs) in the HEKa (**Fig. 2a**). Similarly, we observed a 6.64% population of CSCs and 92.6% non-CSCs from the ACSCC1 cell line (**Supplementary Fig. 7a & b**). To assess the self-renewal capacity of isolated skin CSCs, we performed the spheroid formation assay. Our data revealed an increase in the formation of spheroids in skin CSCs as compared to non-CSCs in the A3886 (**Fig. 2b & c**) and ACSCC1 cell

ARTICLE IN PRESS

lines (**Supp Fig. 7c & d**). Furthermore, we have also performed the IFA assay using the CD133 marker in spheroids from skin CSCs and non-CSCs, which showed increased expression of CD133 in skin CSCs as compared to non-CSCs (**Supplementary Fig. 8a**). Importantly, an *in vivo* serial transplantation assay is the gold standard assay to confirm the presence of CSCs in both skin and oral SCC. Therefore, we performed a serial transplantation assay by subcutaneously injecting 20,000 skin CSCs (1st serial transplantation) into NOD/SCID mice, which formed tumor within 3-4 weeks. Subsequently, 20,000 skin CSCs were isolated from the tumour arising from the 1st transplant and injected subcutaneously into NOD/SCID mice (2nd serial transplantation), which formed tumors within 2-3 weeks. Furthermore, 20,000 skin CSCs isolated from the tumor arising from the 2nd transplant were injected subcutaneously into NOD/SCID mice (3rd serial transplantation) (**Fig. 2d & e, Supplementary Fig. 7e & f**). Our FACS data showed an enrichment of skin CSCs after 3rd serial transplantation, thereby confirming the presence of CSCs (**Supplementary Fig. 8c & d**). To strengthen our data, we performed IFA using the SOX2 marker on serially transplanted skin CSCs tumours. Our data demonstrated an increased number of SOX2+ve cells in skin CSCs tumors, suggesting enrichment of skin CSCs in the serially transplanted tumors (**Supplementary Fig. 8e & f**).

To dissect the molecular signaling in skin CSCs, we performed RNA sequencing on skin CSCs from the A3886 and ACSCC1 cell lines, and non-CSCs of HEKa as a control (**Supplementary Fig. 7g & h**). Our RNA sequencing data showed significant upregulation of non-canonical Wnt ligand (*WNT7B),* EMT markers (*VIMENTIN, TWIST1, ZEB1, ZEB2, SNAI1, SNAI2),* and glycolytic genes (*SLC2A1, SLC2A2, HK2, LDHA*) in the skin CSCs as compared to the non-CSCs (**Fig. 2f & Supplementary Fig. 7i**). Furthermore, to understand the changes in the non-canonical Wnt signaling pathway, we performed the western blot analysis of skin CSCs (A3886) and non-CSCs (A3886). We observed upregulation in expression of non-canonical Wnt signaling, such as WNT7B, DVL2, RAC1, JNK, c-FOS, c-JUN, and SOX2 in CSCs as compared to non-CSCs (**Fig. 2h & i**). To understand the glycolytic rate, we performed Seahorse analysis in CSCs and non-CSCs. The data revealed upregulation of glycolytic flux in CSCs as compared to non-CSCs (Fig. 2g). Moreover, increased glycolytic flux enhanced LDH activity in skin CSCs as compared to non-CSCs (**Fig. 2j**).

Our results indicated that skin CSCs from both cell lines exhibited increased tumorigenic potential *in vivo*, non-canonical Wnt signaling, and glycolysis (2-3-fold as compared to cancer cells, i.e.,

ARTICLE IN PRESS

non-CSCs). The data from skin CSCs of both cell lines are in agreement with findings from human skin SCC patient samples.

- **Loss of Sfrp1 in murine and human skin SCC cell line enhance non-canonical Wnt signaling:** Previously, we reported that Sfrp1-/- skin CSCs showed an increased tumorigenic potential, while the expression profile (Microarray) of Sfrp1-/- skin CSCs revealed the upregulation in expression of stemness, EMT, and proliferation markers as compared to WT skin CSCs[19]. However, the in-depth molecular mechanism by which Sfrp1-/- skin CSCs increase *in vivo* tumorigenesis is yet to be deciphered.

  To delineate a deeper understanding of the molecular mechanism of non-canonical Wnt signaling, we used a two-stage chemical-induced (DMBA/TPA) skin carcinogenesis model in wild-type (WT) (Sfrp1+/+), Sfrp1 heterozygous (Sfrp1+/-), and Sfrp1 homozygous knockout (Sfrp1-/-) mice as described previously[19]. We administered DMBA and TPA to WT, Sfrp1+/-, and Sfrp1-/- mice at various postnatal days (**Supplementary Fig. 9a & b**). IFA analysis of Sfrp1-/- SCC tumors showed the co-expression of epithelial KERATIN14 (K14) and the mesenchymal marker VIMENTIN (**Fig. 3a & c**). Additionally, we isolated CSCs (Lin-/EpCam+/CD34+α6-integrin+) from WT SCC, Sfrp1+/- SCC, and Sfrp1-/- SCC tumors. Our data confirmed that Sfrp1-/- CSCs showed an increased expression of K14 and VIMENTIN as compared to WT CSCs and Sfrp1+/- CSCs (**Fig. 3b-e**). Thus, these data suggested that the loss of SFRP1 facilitated the hybrid EMT phenotype in both murine skin CSCs and tumors.

  Furthermore, to validate our findings in the human context, we used a human skin SCC cell line (A3886). We observed that basal expression of *SFRP1* was absent in the A3886 as compared to HEKa (**Supplementary Fig. 9d**). Our data showed that the loss of *SFRP1* did not show any redundancy in the Sfrp1-/- skin SCC tumors and skin SCC cell line (A3886) (**Supplementary Fig. 9c-e**). We showed an upregulation in expression of the non-canonical ligand *Wnt7b* in the *in vivo* Sfrp1-/- SCC tumors as compared to WT and Sfrp1+/- skin SCC tumors and *in vitro* skin SCC cell line (A3886) as compared to HEKa (**Fig. 3f & g**). Furthermore, we observed upregulation in expression of non-canonical Wnt signaling, such as WNT7B, DVL2, RAC1, JNK, c-FOS, c-JUN, and SOX2, in Sfrp1-/- skin SCC tumors and A3886 (**Fig. 3i-l**).

  Importantly, our *in-silico* analysis by JASPAR showed that the c-*JUN* transcription factor motif had a binding site on the *SOX2* promoter (**Supplementary Fig. 9f and g**). To validate these

ARTICLE IN PRESS

findings, we performed ChIP-qPCR in A3886, which revealed *c-JUN* enrichment at the *SOX2* promoter in the A3886 cell line (**Fig. 3h**).

Furthermore, Sfrp1-/- SCC skin tumors showed a hybrid EMT and increased non-canonical Wnt signaling (WNT7B, DVL2, RAC1, JNK, c-FOS, c-JUN). JNK may regulate adherens junction formation by forming the E-CADHERIN/β-CATENIN complex on the cell surface in the human neonatal primary keratinocytes[29]. Our data demonstrated that Sfrp1-/- skin SCC tumors showed a decreased co-localization of E-CADHERIN/β-CATENIN on the membrane as compared to Sfrp1+/- SCC tumors and WT SCC tumors (**Supplementary Fig. 10a-d**), which suggested that JNK may not only regulate β-CATENIN in adherens junction but also regulate the cytoplasmic pool of β-CATENIN, which translocates to the nucleus. Furthermore, we generated shRNA-mediated inducible knockdown of JNK in A3886 (**Supplementary Fig. 10e & f**). JNK knockdown restored the E-CADHERIN, β-CATENIN, and LEF1 levels in the inducible A3886 shJNK (JNK knockdown) as compared to A3886 VC (Vector control) (**Supplementary Fig. 10g & h**). Additionally, to determine nuclear β-CATENIN activity, we have performed a TOP/FOP Flash assay. We observed a significant upregulation of luciferase activity in A3886 shJNK as compared to A3886 VC (**Supplementary Fig. 10i**), suggesting that the cytosolic pool of β-CATENIN was degraded and unable to translocate to the nucleus in A3886 VC. Similarly, IFA analysis showed the restoration of E-CADHERIN/β-CATENIN localization on the membrane of A3886 shJNK as compared to A3886 VC (**Supplementary Fig. 11a-e**).

Overall, we observed that murine skin SCC tumours and a human skin SCC cell line (A3886) exhibited increased *in vivo* tumorigenic potential, stemness, and hybrid EMT due to enhanced non-canonical Wnt signalling. Furthermore, the non-canonical Wnt pathway regulates canonical Wnt signaling in murine and human skin SCC by increasing JNK levels, which not only affects cell-cell adhesion on the membrane via E-CADHERIN/β-CATENIN but also degrades cytoplasmic β-CATENIN.

ARTICLE IN PRESS

- **Reversal of Sfrp1 overexpression in the human skin SCC cell line showed a decrease *in vivo* tumorigenic potential:**

  To understand the effect of Sfrp1 on *in vivo* tumorigenesis and the metastatic potential, we overexpressed Sfrp1 in the human skin SCC cell line (A3886). We observed a 2.5-fold upregulation in levels of Sfrp1 in the A3886 Sfrp1 overexpressed cell line (A3886 Sfrp1 OE) as compared to A3886 VC. Furthermore, to understand the effect of Sfrp1 overexpression on *in vitro* cell proliferation, we performed clonogenic and BrdU cell proliferation assays. We observed a decrease in the colony-forming efficiency (**Supplementary Fig. 12a & b**) and percentage of BrdU+ve cells in A3886 Sfrp1 OE as compared to A3886 VC (**Fig. 4a & b**). Furthermore, our cell cycle analysis showed a significant downregulation of the S phase in A3886 Sfrp1 OE as compared to A3886 VC (Supplementary Fig. 12c & d), suggesting that the delay in cell cycle decreases in vitro cell proliferation of A3886 Sfrp1 OE as compared to A3886 VC. To check the effect of Sfrp1 overexpression in *in vivo* tumorigenesis, we performed *in vivo* tumorigenic potential by injecting A3886 VC and A3886 Sfrp1 OE cell line subcutaneously into NOD/SCID mice. We observed that A3886 Sfrp1 OE showed a decreased tumorigenic potential as compared to A3886 VC (**Fig. 4c & d**). Furthermore, we demonstrated reduced non-canonical Wnt signaling in A3886 Sfrp1 OE as compared to the A3886 VC (**Fig. 4e & f**). We detected reduced EMT signatures such as VIMENTIN, TWIST1, KERATIN8, and the stemness marker SOX2 in the A3886 Sfrp1 OE tumor as compared to A3886 VC tumors (**Fig. 4g-h**). Moreover, we showed that the *c-JUN* transcription factor motif was strongly enriched at the *SOX2* promoter in A3886 VC. However, Sfrp1 overexpression reduced *c-JUN* enrichment at the *SOX2* promoter region, thereby reducing the stemness of A3886 (**Fig. 4i**). Interestingly, we revealed that Sfrp1 overexpression led to a reduction in the enrichment of *c-JUN* family transcription factors at the chromatin regions of EMT markers such as *VIMENTIN and TWIST1*, Cell cycle-related genes *CCNE1* and *CDK6* and the stemness marker *SOX2* (**Fig. 4i).**

  Similarly, to understand the effect of Sfrp1 overexpression in skin CSCs, we have FACS-sorted the skin cell line A3886 VC CSCs and A3886 Sfrp1 OE CSCs. Our data showed a reduction in the A3886 Sfrp1 OE CSCs as compared to A3886 VC CSCs (**Fig. 5a & b**), which resulted in a decreased spheroid formation capacity of A3886 Sfrp1 OE CSCs (**Supplementary Fig. 12e & f**). Furthermore, we showed that A3886 Sfrp1 OE CSCs exhibited a significant reduction in *in vivo* tumorigenic potential as compared to A3886 VC CSCs (**Fig. 5c & d**).

ARTICLE IN PRESS

Furthermore, A3886 Sfrp1 OE CSCs showed a decrease in hybrid EMT as compared to A3886 VC CSCs (**Fig. 5e & f**). The hybrid tumor state has been associated with an increased metastatic potential in circulating tumor cells Intravenous injection (Tail vein) of A3886 Sfrp1 OE CSCs showed a reduction in lung metastasis as compared to A3886 VC CSCs (**Fig. 5g & h**), which suggested that the loss of Sfrp1 enhanced the spontaneous metastasis and formation of tumor colonies in the lungs (**Fig. 5i-l**).

Overall, our data revealed that Sfrp1 overexpression decreased *in vivo* tumorigenic and metastatic potential, as well as hybrid EMT stemness, in human skin CSCs and a skin SCC cell line, due to reduced non-canonical Wnt signalling.

- **Reversal of Sfrp1 overexpression in the human oral SCC cell line showed decreased tumorigenic and metastatic potential:**

We observed that the upregulation in levels of non-canonical Wnt signaling led to an increase *in vivo* tumorigenic and metastatic potential in murine and human skin SCC. Furthermore, to extrapolate our findings in the oral SCCs, we used the oral SCC cell lines (ACOSC3, ACOSC4, and ACOSC16)[30]. We observed that all the oral SCC cell lines showed a decrease in the Sfrp1 expression (ACOSC3 ~50% reduction, ACOSC4 ~98% reduction, and ACOSC16 ~80% reduction) as compared to primary normal human keratinocytes (HOK)(**Supplementary Fig. 12g**). Therefore, we overexpressed Sfrp1 in all three oral SCC cell lines. To decipher the molecular mechanism in human oral SCC cell lines, we assessed the status of non-canonical Wnt signaling across all oral SCC cell lines. Our western blot data demonstrated that Sfrp1 overexpression resulted in reduced non-canonical Wnt signaling in all oral SCC cell lines (**Fig. 6a & b**). To understand the effect of Sfrp1 overexpression on tumor growth, we assessed the *in vivo* tumorigenic potential by subcutaneously injecting all three oral SCC cell lines into NOD/SCID mice. Our tumorigenesis data showed a reduced tumorigenic potential due to the Sfrp1 overexpression in all three oral SCC cell lines (**Fig. 6c & d**).

Additionally, we performed ChIP-qPCR to determine the enrichment of c-JUN transcription factor at the SOX2 promoter. We found that Sfrp1 overexpression decreased the expression of c-*JUN* and thereby reduced the enrichment at the *SOX2* promoter and the tumor stemness in the oral SCC cell lines (**Fig. 6e**). We validated our findings in the oral CSCs, we have performed the Real-Time PCR of non-canonical Wnt signaling and EMT markers in oral CSCs and non-CSCs. Our data exhibited

ARTICLE IN PRESS

a reduction of Sfrp1 expression in oral CSCs as compared to non-CSCs, which led to enhanced non-canonical Wnt signaling (*WNT7B, DVL2)*, stemness marker *SOX2*, EMT markers such as *VIMENTIN, TWIST1, ZEB1, ZEB2,* and *SNAI1* in all three oral CSCs as compared to non-CSCs (**Supplementary Fig. 12h**). Furthermore, EMT signatures are often associated with increased metastatic potential *in vivo* systems. Our PET-CT results revealed that Sfrp1 overexpression decreased metastatic potential of all the human oral SCC cell lines (**Fig. 6f**).

Furthermore, we have also performed quantitative comparison of gene signatures between skin CSCs and oral CSCs. Our quantitative comparison of EMT markers revealed the expression of *ZEB2* (**1036.9%**), *TWIST1* (**941.8%**), *VIMENTIN* (**688.2%**) and *ZEB1* (**360%**) showed increased expression in the skin CSCs as compare to the oral CSCs (**Supplementary Fig. 4b)**. Furthermore, we observed the upregulation in expression of non-canonical Wnt signaling genes *WNT7B* (**170.6%**), *DVL2* (**65.6%**), and *SOX2* (**9%**) in skin CSCs as compared to oral CSCs (**Supplementary Fig. 4b)**. Moreover, our data revealed the upregulation in expression of glycolytic genes *SLC2A2* (**788%**), *SLC2A1* (**152.8%**), *HK2* (**43.2%**) in skin CSCs as compare to oral CSCs and the upregulation in expression of *LDHA* (**22.6%**) in oral CSCs as compared to skin CSCs (**Supplementary Fig. 4b)**.

Altogether, these data were in congruence with the human skin and oral SCC patient samples, murine skin tumor, and human skin CSCs. The results showed that human oral SCC cell lines and oral CSCs also exhibited increased non-canonical Wnt signaling, *in vivo* tumorigenic potential, and metastatic potential.

ARTICLE IN PRESS

- **Epigenetic regulation of non-canonical Wnt signaling in human skin and oral SCC**

We observed an increased in vivo tumorigenic potential, EMT markers, metastatic potential, and non-canonical Wnt signaling in human skin and oral SCC cell lines. However, the mechanism underlying the loss of Sfrp1 in the skin and oral SCC remains unknown. RNA sequencing data of skin CSCs showed enrichment of PRC2-mediated histone and DNA methylation (**Fig. 7a**). Furthermore, we found that upregulation in expression of the epigenetic modifiers, such as *EZH2, EED, SUZ12, DNMT3A, DNMT3B,* and *HDAC2* in human skin CSCs (**Fig. 7b**) and oral CSCs (**Supplementary Fig. 13a**). Our quantitative comparison between skin and oral CSCs revealed an upregulation in expression of epigenetic modifiers *DNMT3A* (**17.1%**), *DNMT3B* (**17%**), and *EZH2* (**25.8%**) in the oral CSCs as compared to skin CSCs (**Supplementary Fig. 4b).** To

ARTICLE IN PRESS

understand the levels of epigenetic modifiers, we performed western blot analysis of advanced-stage skin SCC patients, which showed an upregulation of EZH2 levels, followed by increased histone methylation (H3K27me3) as compared to normal skin (adjacent margin) (**Supplementary Fig. 2c & d**). Similarly, our IHC data showed an increased level of EZH2 in skin SCC samples as compared to normal skin (adjacent margin) (**Fig. 7c & d**) and oral SCC patients as compared to normal oral mucosa (adjacent margin) (**Fig. 7e & f**). We demonstrated that high EZH2 expression is associated with poor OS in patients with skin and oral SCC patients (**Supplementary Fig. 13b & c**) (**Supplementary Fig. 3d)**.

Additionally, our *in-silico* analysis revealed EZH2 binding to the Sfrp1 promoter region (**Supplementary Fig. 13d & e**). Our ChIP-qPCR data showed that *EZH2* binds to the promoter region of *SFRP1* and regulates its expression in the skin and oral SCC cell lines (**Supplementary Fig. 2e & f**). EZH2 belongs to the PRC2 complex family and methylates H3 at the K27 position by recruiting various DNMTs (DNA methyltransferases). To understand the *SFRP1* promoter hypermethylation, we performed ChIP-qPCR analysis, which showed that the H3K27me3 mark was significantly upregulated around the SFRP1 promoter region in human skin and oral SCC cell lines (Fig. 7g **& j)**. Moreover, western blot analysis revealed the upregulation of EZH2 levels in skin and oral SCC cell lines, which led to upregulation in the global levels of histone methylation (H3K27me3) and reduction of histone acetylation (H3K27ac) in human skin and oral SCC cell lines (**Fig. 7h, i, k, l**).

Overall, our data suggested that histone and DNA methylation play vital roles in the loss of Sfrp1 and modulate the non-canonical Wnt signaling in skin and oral SCC.

- **DAC reduces histone methylation and restores the SFRP1 levels in skin and oral SCC cell lines:**

We demonstrated that the epigenetic modifier EZH2 recruited DNMTs, which enhanced promoter hypermethylation and promoted the loss of SFRP1, thereby increasing non-canonical Wnt signaling in skin and oral SCC cell lines. Therefore, we used the pharmacological drug DAC, a methyltransferase inhibitor that is being used in clinical trials of Acute Myeloid Leukemia (AML)[31,32]. To assess the effect of DAC on Sfrp1 promoter hypermethylation in A3886 and A3886+DAC, we performed the ChIP-qPCR. We observed decreased histone levels (H3K27me3) (**Fig. 8a**) and increased levels of histone acetylation (H3K27ac) on the Sfrp1 promoter after DAC

ARTICLE IN PRESS

treatment in the skin SCC cell line (**Supplementary Fig. 13f**) and oral SCC cell lines (**Fig. 8b** & **Supplementary Fig. 13g**). Moreover, to understand the effect of DNA methylation after DAC treatment, we performed ChIP-qPCR using 5-methyl cytosine (5-mc) in human skin and oral SCC cell lines. Our data revealed that DAC treatment reduced 5-mc on the Sfrp1 promoter, thereby decreasing hypermethylation in skin and oral SCC cell lines (**Supplementary Fig. 13h & i**). Similarly, we performed western blot analysis of histone methylation and acetylation levels in human skin and oral SCC cell lines. Our data revealed a decrease in H3K27me3 and an increase in levels of H3K27ac after DAC treatment, suggesting the restoration of Sfrp1 expression in human skin and oral SCC cell lines (**Fig. 8c-f).** Overall, we observed that DAC treatment restored SFRP1 levels, thereby decreasing non-canonical Wnt signaling in skin and oral SCC cell lines.

We have observed that epigenetic modification increases in non-canonical Wnt signaling, the stemness marker *SOX2,* and EMT markers in skin and oral SCC cell lines. Our RNA sequencing data on skin CSCs showed the enrichment of hypoxia-inducible factor (HIF1α) (**Fig. 8g**). To understand the correlation between stemness and hypoxia, we performed promoter analysis, which showed that SOX2 regulates HIF1α by binding to the promoter. Our ChIP-qPCR result showed that *SOX2* binds to the promoter region of *HIF1α* in skin and oral SCC cell lines. However, DAC treatment restored SFRP1 expression and reduced SOX2 enrichment at the *HIF1α* promoter, thereby reducing hypoxia in the skin and oral SCC cell lines (**Fig. 8h & i**).

ARTICLE IN PRESS

- **DAC reduces glycolysis through non-canonical Wnt signaling:**

We have observed an increase level in histone methylation, leading to the loss of SFRP1, which enhanced non-canonical Wnt signaling and hypoxia in skin and oral SCC. However, the regulation of metabolic reprogramming due to epigenetic modification and non-canonical Wnt signaling remains elusive. To uncover the crosstalk between non-canonical Wnt signaling, hypoxia and glycolysis, we analyzed the RNA sequencing and GSEA (gene set enrichment analysis) analysis of human skin CSCs, which exhibited the enrichment of glycolytic genes (*SLC2A1, SLC2A2, HK2, ENO1*) (**Fig. 8j & Supplementary Fig. 14a**). However, DAC treatment reduced the expression of glycolytic genes (**Supplementary Fig. 14b**) Furthermore, our seahorse experiment also showed an increased glycolytic rate in skin and oral SCC cell lines as compared to normal skin and oral keratinocytes (**Supplementary Fig. 14c & d**). Additionally, our Real-time PCR data exhibited the upregulation in expression of *SLC2A1, SLC2A2, LDHA, LDHB,* and *SIRT2* in human skin and oral

ARTICLE IN PRESS

CSCs as compared to non-CSCs (**Supplementary Fig. 14e & f**). Our STRING analysis revealed that hypoxia (*HIF1α)* regulates the expression of glycolytic genes (*HK2, LDHA, SLC2A2)* (**Fig. 8k**). To validate the regulation of *HK2, LDHA,* and *SLC2A2* by *HIF1α,* we performed ChIP-qPCR. Our data showed that *HIF1α* strongly bound to the promoters of HK2 and LDHA, whereas it bound weakly to the *SLC2A2* promoter. However, DAC treatment reduced the enrichment of *HIF1α* at the promoter regions of HK2, LDHA, and SLC2A2 in both human skin and oral SCC cell lines (**Fig. 8l & m**). Furthermore, our western blot analysis also showed a reduction in HIF1α, HK2, and LDHA levels after DAC treatment in human skin and oral SCC cell lines (**Fig. 9a-d**). Interestingly, DAC treatment reduced LDH activity (**Fig. 9e & i**) and the substrate levels of pyruvate and lactate (**Fig. 9f, g, j, k**), while an increase in the substrate levels of Acetyl-CoA was observed in human skin (**Fig. 9h**) and oral SCC cell lines (**Fig. 9l**).

Overall, our data unraveled a mode of action of DAC treatment, which restored SFRP1 levels, reduced c-Jun/Sox2/Hif1α axis, non-canonical Wnt signaling and metabolic reprogramming, thereby decreasing cancer stemness and the *in vivo* tumorigenic and metastatic potential of human skin and oral SCC.

- **Pharmacological drug DAC and RAC1i decrease *in vivo* tumorigenic potential in the skin and oral SCC cell lines:**

  Our data showed that DAC treatment decreased global hypermethylation and reduced *in vivo* tumor growth of skin (~50% reduction) (**Fig. 10a & b**) and oral SCC (~50% reduction) (**Fig. 10c & d**). Additionally, we observed that Sfrp1 overexpression reduced non-canonical Wnt signaling, thereby decreasing the in vivo tumorigenic potential of skin and oral SCC. Furthermore, to assess the combinatorial effect of targeting epigenetic modification and non-canonical Wnt signaling in skin and oral SCC, we used DAC and RAC1i. We have injected 1 x 10^6 skin and oral SCC cell lines subcutaneously into the flank of NOD/SCID mice. Once the tumour reached a volume of 150 mm^3, we treated the NOD/SCID mice with RAC1i alone or in combination of DAC. Our data revealed that treatment with only RAC1i reduced tumor volume by ~50-55% in skin and oral SCC. However, with the combination treatment of DAC and RAC1i reduced tumor volume by ~75-80% in the skin (**Fig. 10e & f**) and in oral SCC (**Fig. 10g-j**).

  To understand the detailed molecular mechanism following DAC and RAC1i, we performed RNA sequencing on DAC-treated skin SCC cell lines, RAC1i-treated skin SCC cell lines, and the skin

ARTICLE IN PRESS

SCC cell lines treated with a combination of DAC & RAC1i. (**Supplementary Fig. 15a-d**). Our RNA sequencing data of DAC treatment showed an increased expression of *SFRP1*, while reduction in levels of epigenetic modifiers (*EZH2, DNMT1, DNMT3A, HDAC2, & HDAC10*), non-canonical Wnt signaling (*WNT7B*), EMT markers (*VIMENTIN, TWIST1, ZEB1, ZEB2*), and genes involved in regulating glycolysis (*SLC2A1, SLC2A2, HK2, ENO1, SIRT2, SIRT7*) (**Supplementary Fig. 14b & 15e**). Furthermore, we observed that RAC1 inhibition decreased the expression of stemness marker (*SOX2*) and glycolytic genes (*SLC2A1, SLC2A2, HK2, ENO1, SIRT2, SIRT7*). Similarly, we have observed that a combination of DAC and RAC1i reduced DNA methylation, which in turn increased SFRP1 expression and reduced glycolysis in the skin SCC cell line (**Supplementary Fig. 14b & 15e**).

Overall, the data suggested that the therapeutic effects of DAC and RAC1i target the crosstalk among epigenetic modification, non-canonical Wnt signaling, and metabolic reprogramming, thereby reducing the *in vivo* tumorigenic potential of skin and oral SCC (**Fig. 10k**).

ARTICLE IN PRESS

ARTICLE IN PRESS

3. Discussion:

In this study, we sought to understand the molecular mechanisms involved in epigenetic modification, non-canonical Wnt signaling, and metabolic reprogramming in skin and oral SCC. Our RNA sequencing analysis of advanced-stage skin CSCs revealed that key epigenetic modifiers were upregulated, leading to a decrease in SFRP1 levels and the activation of the non-canonical Wnt signaling pathway. Similarly, in our patient cohort of advanced-stage skin and oral SCC, we found a negative correlation between SFRP1 and the expression of EZH2, WNT7B, and c-JUN, which was associated with poor OS in advanced-stage skin and oral SCC patients. Previous studies have demonstrated that hypermethylation of H3K27me3 inhibits SFRP1 expression, thereby facilitating cell proliferation via the Wnt/β-catenin signaling pathway in esophageal squamous cell carcinoma[33]. Furthermore, DACT3, a negative regulator of Wnt/β-catenin signaling, was transcriptionally repressed due to histone methylation (H3K27me3 and H4K20me3) in colorectal cancer[34]. Moreover, abnormal H3K27ac activates the Wnt/β-catenin and PI3K/Akt pathway that promote the EMT in gastric cancer[35]. Overall, these mechanisms emphasize the crucial roles of epigenetic modifications in regulating signaling pathways during tumor progression. Similarly, in our study, we observed that elevated levels of EZH2 contributed to an increase level in histone methylation (H3K27me3) by recruiting the PRC2 complex and DNMTs (DNMT3a, DNMT3b) in both skin and oral SCC cell lines. Furthermore, ChIP-qPCR data showed that promoter hypermethylation leads to the loss of Sfrp1 expression in both the human skin and oral SCC cell lines. Sfrp1 overexpression in colorectal cancer inhibits cell proliferation, invasion, and migration[36]. Sfrp1 overexpression reduces *in vivo* tumorigenesis by targeting Wnt/β-catenin in ovarian cancer[37]. In contrast, Sfrp1 overexpression showed increased cell proliferation and angiogenesis in gastric cancer[38] and enhanced prostate CSCs properties *in vitro*[39]. Furthermore, the regulation of *Wnt7b* by *Sfrp1* or *Sfrp2* during early mouse embryogenesis[12]; *Wnt7b* expressed in the mouse hippocampus activates the *Dvl2, Rac*, and *Jnk* in the neuronal hippocampus[40]. Moreover, WNT7B promoted differentiation and migration by activating c-JUN in human dental cells.[41] WNT7B overexpression is associated with poor OS in prostate cancer[42]. The epigenetic modification of the non-canonical Wnt ligand (Wnt5a) leads to an increase in Cyclin-D1 expression, which is associated with poor OS in AML[43]. However, the precise molecular mechanisms by which histone and DNA methylation regulate non-canonical Wnt signaling have yet to be explored in SCC.

ARTICLE IN PRESS

To understand in-depth molecular mechanisms, we performed topicaly administered of the chemical carcinogen DMBA/TPA to Sfrp1-/- mice. We assessed different Wnt ligands in murine and human skin SCC and observed upregulation in expression of the non-canonical Wnt ligand *WNT7B* in murine skin SCC tumors and human skin SCC cell lines. Importantly, the loss of Sfrp1 increased expression of non-canonical Wnt signaling pathway (WNT7B, DVL2, RAC1, JNK, c-FOS, c-JUN) and stemness marker (SOX2) in murine and human skin SCC. SOX2 transcription factor in neural stem cells regulates the Ap1 transcription factor[44]; *c-JUN* and *c-FOS* genes regulated stemness markers Nanog, *Oct3/4*, and *Sox2* in colorectal cancer[45], while *Sox2* deletion reduced tumor formation in skin SCC[46]. Similarly, our ChIP-qPCR data in skin SCC revealed that c-*JUN* binding to the promoter regions of *SOX2*, *VIMENTIN*, *TWIST1*, *ZEB1*, *CCNE1*, and *CDK6* indicated that the non-canonical Wnt signalling pathway regulates tumor stemness, EMT, and cell proliferation. Moreover, RNA sequencing data on human skin CSCs showed an increased expression of *WNT7B* ligand, stemness marker *SOX2*, epithelial markers, and mesenchymal markers in human skin CSCs as compared to non-CSCs, suggesting both epithelial and mesenchymal phenotypes in the human skin CSCs.

The hybrid EMT populations have been characterized by the co-expression of epithelial and mesenchymal markers in the genetically induced murine skin SCC[47]. FAT1 mutation in genetically induced skin SCC tumors acquired the hybrid EMT phenotype[48] that occurred very late during the tumor progression, which showed high tumorigenic and metastatic potential[49]. Moreover, breast cancer stem-like cells showed increased tumorigenesis and invasion due to the hybrid EMT phenotype[50]. The hybrid EMT state of tumor cells possesses higher metastatic potential upon intravenous injection in NOD/SCID mice[49]. In our study, Sfrp1-/- SCC tumors showed the expression of K14 and VIMENTIN in the keratin pearls, which indicated signs of squamous differentiation and stable hybrid EMT phenotypes in Sfrp1-/- skin SCC tumors. Similarly, Sfrp1-/- CSCs exhibited increased hybrid EMT as compared to Sfrp1+/- CSCs and WT CSCs, suggesting that Sfrp1-/- CSCs possess higher tumorigenic potential.

Additionally, JNK may regulate β-CATENIN on the cell surface in the human neonatal primary keratinocytes[29]. Similarly, we also observed that upregulation in levels of non-canonical Wnt signaling reduces canonical Wnt signaling by decreasing the E-CADHERIN and β-CATENIN levels on the membrane due to JNK in the murine skin SCC (Sfrp1-/- SCC) and human skin SCC cell line, which results in the disruption of the apical and basal cell surface junctions formed by E-

ARTICLE IN PRESS

CADHERIN/β-CATENIN due to the phosphorylation of β-CATENIN leads to its degradation. Therefore, upregulation in levels of non-canonical Wnt signaling exhibited the decoupling of cell adhesion and decreased canonical Wnt signaling, which may contribute to metastasis in murine and human skin SCC.

Importantly, we observed that histone and DNA methylation are key regulators of Sfrp1 promoter hypermethylation, which, in turn, activates the non-canonical Wnt signaling pathway in skin and oral SCC. These findings highlighted the critical role of hypermethylation in modulating signaling pathways associated with tumor progression.

DNA methylation also promotes metabolic reprogramming in cancer cells. Hexokinase-2 (HK2) upregulation in expression due to promoter hypomethylation increased glycolytic flux in glioblastoma[51]. In bladder cancer, the upregulation in expression of glycolytic genes is due to demethylation of H3K9me2[52]. Several reports have indicated that canonical Wnt signaling also enhanced metabolic reprogramming in different cancers[25,27,53]. Wnt/β-catenin negatively regulates the expression of FOXA1, thereby modulating amino acid metabolism in liver cancer[27]. Furthermore, α-ketoglutarate decreases Wnt signaling by enhancing glutamine metabolism in colorectal cancer[53]. Overall, it is observed that either epigenetic modification can either modulate glycolysis or canonical Wnt signaling regulates metabolic reprogramming in SCC. However, the crosstalk between epigenetic modification and non-canonical Wnt signaling and its regulation of metabolic reprogramming remains poorly understood. In our study, we showed that *c-JUN* regulates the expression of stemness marker *SOX2* by binding to the SOX2 promoter, which, in turn, controls hypoxia-inducing factor HIF1α, thereby enhancing glycolytic genes such as *SLC2A2, HK2,* and *LDHA*. Hitherto, these findings unravelled that not only epigenetic reprogramming modulates the glycolytic pathway, but also the cross-talk between epigenetics and non-canonical Wnt signaling regulates metabolic reprogramming in both skin and oral SCC.

DAC, a methyl transferase inhibitor, eliminated H3K27me3 in adult T-cell lymphoma patients, thereby reprogramming entire cancer epigenome, which showed better clinical outcomes[54]. Furthermore, DAC and DZNep treatment inhibited H3K27me3 in AML cells[55]. DAC rescued cisplatin resistance by reducing methylation in HNSCC[56]. Similarly, RAC1 overexpression showed an increased *in vivo* tumorigenesis and metastasis in several cancers, such as non-small cell lung carcinoma, breast cancer, and gastric cancer[57–59]. RAC1i affects cytoskeleton modelling in different types of cancers[60–63]. Rac1i inhibition (NSC23766) attenuated oncogenic effects

ARTICLE IN PRESS

mediated by LDHA[62]. RAC1i abrogated the CCL2-CCR4 axis in HNSCC cells[60]. Inhibition of RAC1 led to decreased cell proliferation and tumorigenesis in prostate cancer cells[63]. However, no such reports have showed the combination of DAC and RAC1i treatment targets crosstalk among epigenetic modification, non-canonical Wnt signaling, and metabolic reprogramming in the skin and oral SCC.

Understanding the effects of DAC and RAC1i on the skin and oral SCC could provide valuable insights into potential therapeutic strategies. We observed that a treatment with DAC and RAC1i alone reduced tumor growth (~50% reduction) in skin and oral SCC. However, the combination of the DAC and RAC1i reduced tumour volume by ~75-80% in skin and oral SCC, suggesting that targeting global hypermethylation and non-canonical Wnt signalling would be a better therapeutic approach for the treatment of skin and oral SCC.

In conclusion, we uncovered the mode of action of DAC and RAC1i by targeting the c-Jun/Sox2/Hif1α axis, which attenuates cancer stemness, tumor growth, and metastasis, leading to a reduction in glycolytic pathway in human skin and oral SCC.

Altogether, our study revealed crosstalk between epigenetic regulation that drives non-canonical Wnt signaling, followed by the regulation of metabolism. These findings have profound clinical implications, suggesting that targeting these pathways could support personalized treatment strategies for patients with loss of SFRP1 expression that may potentially improve patient outcomes.

ARTICLE IN PRESS

ARTICLE IN PRESS

4. Methods:

➢ Animal ethical regulations:

Our study protocol was approved by the ACTREC-TMC, Institutional Animal Ethics (IAEC), project #12/2021 (April 2021). Our IAEC adhered to the CPSEA criteria set by the Indian Ministry of Environment and Forests for conducting all animal research. In addition, we adhered to the Arrive criteria and the requirements for care and animal welfare set by the National Research Council in Washington, DC. We monitored the mice daily and euthanized them if the tumor reached the specified endpoint size of 20 mm in diameter or if the tumor became ulcerated, regardless of size. We euthanized the animal if a mouse lost more than 20% of its initial body weight or exhibited signs of distress based on overall health and spontaneous activity levels. The studies conducted in this research did not exceed the maximum tumor size limit (20mm diameter). Our animal house facility is fully compliant with ethical standards. The ambient temperature was maintained at 25°C, with humidity around 55% (±15%) in the mouse cage. Each animal cage contained sustenance, hydration, and two types of nesting materials. A 12:12 semi-natural light cycle was used.

➢ Mouse strains:

Sfrp1 knockout mice were provided as a kind gift by Dr. Akihiko Shimono[12]. To generate mice with a heterozygous deletion of the Sfrp1 gene (Sfrp1+/-), we crossed homozygous knockout mice (Sfrp1-/-) with wild-type C57BL/6 mice. We then bred the resulting Sfrp1+/- heterozygous mice to Sfrp1-/- homozygous mice to obtain three genotypes: wild-type (WT) (Sfrp1+/+), heterozygous (Sfrp1+/-), and homozygous knockout (Sfrp1-/-). We used mice from the same litter for all the experiments. Additionally, we have obtained all NOD/SCID mice from the ACTREC animal facility for in vivo tumorigenesis, serial transplantation, and metastasis experiments.

➢ Chemical-induced DMBA/TPA carcinogenesis model:

We have used a two-stage chemical-induced skin carcinogenesis in wild-type (WT), Sfrp1 heterozygous (+/-), and Sfrp1 homozygous knockout (-/-) individual mice as described previously[19,64]. We shaved the mice on postnatal day 22 (PD22) and treated them with 195nmol of DMBA (9,10-dimethyl-1,2-benzanthracene) per animal on three days: PD23, PD25, and PD27. DMBA induces the mutations (*Hras1* & *Tp53*) in the mice. Furthermore, we administered 4nmol of TPA (12-O-tetradecanoyl phorbol-13-acetate; Cat no: P8139, Sigma) per animal twice a week until they were euthanized. We tracked tumor initiation, number of tumors per mouse, and tumor size throughout the experiment. We assessed tumor volumes on the day of onset and at weekly

ARTICLE IN PRESS

intervals until the tumors reached 20mm in diameter. We assessed the tumor volume using a vernier caliper. We calculated tumor volumes using the formula: $V = 0.5 \times (L \times W^2)$, where L represents the minor tumor axis and W represents the major tumor axis.

- **Tumor harvesting and single-cell suspension culture:**

  We have harvested tumors from murine skin and performed single-cell suspension culture as described previously[19]. Tumors were collected in cold 1X PBS for tumor digestion. The tumor specimens were minced in 1X PBS and subsequently immersed in a solution of 0.25% trypsin-EDTA (Cat no: T4799, Sigma). Furthermore, the tumor samples were incubated at 4°C overnight in the 0.25% trypsin-EDTA. The following day, minced tumor samples were kept at 37˚C for 15 minutes. The activity of trypsin-EDTA was inhibited using complete DMEM media. The single-cell suspension was collected using a 70µm strainer and then filtered through a 40µm strainer. The cells were collected by spinning them in a centrifuge at 200g for 5 minutes. Furthermore, the pellet was resuspended in Fluorescence-activated cell sorting (FACS) buffer containing 1X PBS and 5% chelated fetal bovine serum.

- **Isolation of CSCs from murine skin SCC tumors:**

  We isolated CSCs using specific markers, such as Lin- (FITC)/Epcam+(PE-Cy7)/α6 integrin (PE)/CD34 (APC), from murine skin SCC tumors[65]. To remove cells from different blood lineages, we used antibodies, including CD45 (excludes all hematopoietic cells except mature erythrocytes and platelets), CD31 (endothelial cells), and CD140a (fibroblasts). Furthermore, we stained the cells using specific antibodies after preparing the single-cell suspension. These included anti-CD45-FITC (Cat no: 103108, Biolegend), anti-CD31-FITC (Cat no: 102406, Biolegend), anti-CD140a-FITC (Cat no: 11-1401-82, eBioscience), and anti-Epcam-PE-Cy7 (Cat no: 118216; BioLegend), anti-mouse CD34 biotin (Cat no: 13-0341-85; bioscience), and anti-α6 integrin-PE (Cat no: 555736; BD Pharmingen). The secondary antibody staining was done using streptavidin-APC (Cat no: 554067; BD Pharmingen). The viable cells were selected based on propidium iodide (PI) staining (Cat no: P4170; Sigma). We removed all cells from different blood lineages using FITC gating, as all the antibodies for each lineage were labeled with FITC. Additionally, we sorted the cells using PE-Cy7 to select EpCAM-positive cells. Furthermore, we sorted the cells using a PE-Mouse IgG2a k isotype control (Cat no: 555574; BD Pharmingen) to identify cells expressing anti-α6-integrin conjugated to PE. Additionally, we used streptavidin-APC to exclude cells exhibiting non-specific binding of the secondary antibody. We have also provided the staining strategy in **Supplementary**

ARTICLE IN PRESS

Table 2. FACS was performed on the FACSAria-III and analysed with FACS FlowJo (BD Bioscience). We collected the FACS-sorted cells in the media and used them for immunofluorescence (IFA). The gating strategy is provided in **Supplementary Fig. 16b.**

- **Human sample collection:**

We collected snap-frozen tumour biopsies from advanced-stage, treatment-naïve oral SCC from the tumour tissue repository of Tata Memorial Centre (TMC)-ACTREC and Tata Memorial Hospital (TMH). We performed IHC of different markers (SFRP1, EZH2, WNT7B, c-JUN) using the retrospectively collected cohort (**n=59**). Our study protocol was approved by the ACTREC-TMC Institutional Ethics Committee (IECIII) for the collection and use of oral SCC tissue samples (Study Protocol #900188). It was conducted in accordance with the Declaration of Helsinki. We have also collected normal oral mucosa tissues (adjacent margin) (n=12) as controls under the study protocol #900188. Additionally, we collected paraffin-embedded blocks (Retrospective samples, n=28) from advanced-stage treatment-naïve and prior-treated skin SCC patients at TMH. Furthermore, we have also collected normal skin tissue as a control under study protocol #900939, which was performed in accordance with the Declaration of Helsinki. Moreover, we collected prospective samples (**n=6**) of advanced-stage, treatment-naïve and prior-treated skin SCC from TMH and ACTREC-TMC. Informed consent was obtained from all the patients. The fresh tumor biopsies were directly collected in a tissue storage solution (Cat no: 130-100-008; Miltenyi Biotec) from the surgery room. We have also collected normal skin tissues (adjacent margin) (**n=10**) as a control under the study protocol #900939. Furthermore, we have performed FACS to sort the CSCs population from fresh tumour biopsies of advanced-stage skin SCC patients. Our study protocol was approved by the ACTREC-TMC Institutional Ethics Committee (IECIII) for the collection and use of the skin SCC tissue samples (Study Protocol #900939). We assigned a unique code to the tumor samples collected from patients, which was used for all subsequent experiments.

- **Isolation of CSCs from the skin SCC patient tumor and normal skin (adjacent margin):**

We collected the tumor biopsies and normal skin (adjacent margin) in a tissue storage solution. The tumors were then sterilized with a 10% iodine solution for 5-10 minutes, followed by three washes with 1X PBS. The tumor was minced, chopped into small pieces, and digested in 0.25% Trypsin-EDTA overnight at 4°C. The following day, tumor samples were incubated at 37°C for 15 minutes, and a single-cell suspension culture was prepared by passing the mixture through 70µm and 40µm filters. Furthermore, the single-cell suspension was washed with 1X PBS, centrifuged at 1000g for

ARTICLE IN PRESS

5 minutes, and resuspended in 500µl FACS buffer (5% FCS in 1X PBS). Next, the single-cell suspension was stained with the antibody mixture of different blood lineage markers anti-CD2-PE (Cat no: 555327; BD Bioscience), anti-CD3-PE (Cat no: 555340; BD Bioscience), anti-CD10-PE (Cat no: 555375; BD Bioscience), anti-CD18-PE (Cat no: 555924; BD Bioscience), anti-CD16-PE (Cat no: 555407; BD Bioscience), anti-CD31-PE (Cat no: 555446; BD Bioscience), anti-CD64-PE (Cat no: 558592; BD Bioscience), anti-CD140b-PE (Cat no: 558821; BD Bioscience) and CSCs marker anti-human-CD133-APC (Cat no: 566597; BD Pharmingen). After the antibody incubation, cells were washed with 1X PBS, centrifuged at 1000g for 5 minutes, and resuspended in 500µl FACS buffer containing propidium iodide (PI). Live cells were gated using PI staining. The isotype controls, anti-human PE IgG2κ (Cat no: 555574; BD Bioscience) and anti-human APC IgG1κ (Cat no: 555749; BD Bioscience), were used to exclude non-specific binding. We FACS-sorted Lin-CD133+ cells as CSCs and Lin- CD133- cells as non-CSCs from both tumor biopsies and normal skin (adjacent margin). We have also provided the detailed staining strategy in **Supplementary Table 1.** We performed FACS sorting using the FACS Aria I or III and analyzed the data with FACS FlowJo software. We FACS-sorted the cells directly into RNA lysis buffer (Cat no: 400791-13, Agilent Technologies) for RNA isolation. The gating strategy is provided in **Supplementary Fig. 16a.**

- **Murine primary cell culture:**

  We FACS-isolated Lin-/EpCAM+/CD34+/α-6 integrin+ (murine skin CSCs) from the WT SCC, Sfrp1+/- SCC, and Sfrp1-/- SCC tumors. We seeded the FACS-sorted cells onto coverslips and cultured them for six hours in E-media supplemented with 15% FBS (Cat no: SH30037.3, Hyclone), 5mg/ml Insulin (Cat no: IPP00, Sigma), Transferrin (Cat no: T2252, Sigma), 4mg/ml hydrocortisone (Cat no: # 386698, Calbiochem), $10^{\wedge-6}$ M cholera toxin (Cat No: # 150005, MP Biochemicals), and 1% antibiotic-antimycotic (Cat no: 15240062, Gibco). The cells were incubated at 37°C, 5% CO_2. Furthermore, we used sorted cells to perform IFA for different markers, such as KERATIN-14 and VIMENTIN.

- **Human cell line culture:**

  We have used the HEKa (Cat no: C0055C, Invitrogen), HOK (Cat no: #2610, Science Cell) as skin and oral control cell lines respectively, and the A3886 skin SCC cell line, a generous gift from Dr. Colin Jamora (Shiv Nadar University, Delhi)[66]. These cell lines were cultured in the DMEM (Cat no: 12800017; Gibco) containing 10% FBS (Cat no: RM10409, Hi-media) and 1% antibiotic

ARTICLE IN PRESS

solution. We have also used the advanced-stage patient-derived skin SCC cell line ACSCC1[67]. Furthermore, we have also used the patient-derived treatment-naïve advanced-stage oral SCC cell lines ACOSC3, ACOSC4, and ACOSC16 established in our laboratory[68]. We cultured all the oral SCC cell lines in MEM (Cat no: 61100061, Gibco) containing 10% FBS (Cat no: 1082147, Gibco), 10% horse serum (Cat no: 26050088, Gibco), and 1% antibiotic solution. We used 0.25% Trypsin-EDTA to passage all the cell lines. The cell lines and primary keratinocytes were maintained in the incubator at 37°C, 5% CO_2.

- **Generation of shRNA-mediated knockdown and overexpression cell lines:**

We have obtained Institutional Biosafety Committee (IBSC) approval to conduct lentiviral work. (Study Protocol number: 04/2019). We have generated the shRNA-mediated knockdown of JNK in the A3886 skin SCC cell line. We have used the 3rd generation lentiviral vector Tet-pLKo-puro (Gift from Dr. Neelam Shirshat; Addgene plasmid Cat no: #21915). The shRNA was designed using the Broad Institute platform (https://portals.broadinstitute.org/gpp/public/seq/search). The generation of the stable knockdown cell line, lentivirus, was produced by Lipofectamine LTX (Invitrogen) transfection in the HEK293FT cells with the shRNA cloned vector and the helper plasmids psPAX2 (Addgene plasmid Cat no: #12260), pMD2.G (Addgene plasmid Cat no: #12259), and pAdvantage vector (Promega). We maintained HEK293FT cells in DMEM with 10% FBS and 1% antibiotic solution. We collected the viral supernatant and filtered it through a 0.45µm filter after 72 hours of transfection. Furthermore, A3886 cells were transfected with the virus and polybrene (4 µg/µl) for 24 hrs. We changed the media and selected the transfected cells using puromycin (1 µg/ml) (Cat. no. P8833, Sigma). After 15 days of selection, doxycycline (1µg/ml) (Cat no: D9891, Sigma) was added to the media for 48 hours to induce the shRNA expression. We used a 1 µg/ml doxycycline concentration (up to 48 hours) for all *in vitro* experiments. Furthermore, we have fed the doxycycline-containing food (Cat. no. S3888, Bioserv) to NOD/SCID mice to induce shRNA expression for the *in vivo* tumorigenesis assay.

We have purchased the Sfrp1-mGFP (Cat no: RC207328L4, Origene) cDNA clone in the Lenti vector for the overexpression of the Sfrp1 protein in the A3886 skin SCC cell line, ACOSC3, ACOSC4, and ACOSC16 oral SCC cell lines. Stable Sfrp1 overexpression cell lines were generated by lentivirus production abovementioned in the protocol. Furthermore, all cells were transfected with the virus and polybrene (4 µg/µl) for 24 hours. We selected the transfected cells based on GFP

ARTICLE IN PRESS

fluorescence and plated them in a 24-well plate. As soon as the single colony was visible, the clone was amplified, and protein was extracted to assess Sfrp1 overexpression.

- **FACS analysis of skin SCC cell line and primary keratinocytes (HEKa):**

  We have used skin SCC cell lines (A3886 and ACSCC1) to sort the CSCs population using the CD133 marker. We have also taken the HEKa cells as a control. We allowed the cells to grow until they reached 80% confluency. We harvested the cells using 0.25% Trypsin-EDTA, washed them with 1X PBS, centrifuged at 1000g for 5 minutes, and resuspended them in 500µl FACS buffer (5% FCS in 1X PBS). We stained the cells with anti-human CD133-PE (Cat no: 566594, BD Bioscience) and incubated them on ice for 30 minutes. Furthermore, we washed the stained cells with 1X PBS, centrifuged at 1000g for 5 minutes, and resuspended them in 500µl FACS buffer containing PI. We selected the viable cells based on PI staining. The isotype control IgG1κ was used for the experiment. We FACS-sorted CD133+ cells as CSCs and CD133- cells as non-CSCs from the skin SCC cell line. We have also sorted the CD133- cells (non-CSCs) from the HEKa. FACS analysis and processing were performed on the FACS Aria I or III using FACS FlowJo software. We FACS-sorted the cells into media and RNA lysis buffer. The FACS-sorted cells were used for spheroid formation, serial transplantation, RNA isolation, and western blot analysis. The gating strategy is provided in **Supplementary Fig. 17a.**

- **FACS analysis of oral SCC cell lines:**

  We have used oral SCC cell lines ACOSC3, ACOSC4, and ACOSC16 to sort the CSCs population. We used CSCs markers such as CD44 and ALDH (aldehyde dehydrogenase). We have allowed all the cells to grow till 80% confluency. We harvested the cells using 0.25% Trypsin-EDTA, washed them with 1X PBS, centrifuged at 1000g for 5 minutes, and resuspended them in 500µl FACS buffer (5% FCS in 1X PBS). Viability staining was performed on the residual suspension employing the Zombie Aqua Fixable Viability kit (Cat no: 423101, Biolegend). In brief, the dye stock was diluted 1:500 in 1X PBS, and the cell suspension was stained with this dilution for 15 minutes at ambient temperature. Subsequently, the cells underwent washing with FACS buffer to terminate the staining process. The cells were incubated on ice for 30 minutes, with gentle tapping to prevent them from pelleting. A wash was given with FACS buffer to tubes, followed by a centrifuge at 1000g for 5 min. The supernatant was discarded, and the pellet was resuspended in 200µl FACS buffer. The pellet was resuspended in 500µl AldeRed buffer. 2µl DEAB reagent was added to the tube. 2µl AldeRed reagent (Cat no: SCR150, Merck) was added to the test tube and given a quick mix by

ARTICLE IN PRESS

gentle tapping. At the end of the incubation, the cells were washed with FACS buffer, then centrifuged at 1000g for 5 minutes. Furthermore, we resuspended the cells in 200µl FACS buffer and added the CD44-APC antibody. The tubes were kept on ice for 30 minutes with gentle tapping every 10 minutes. At the end of the incubation, the cells were washed with FACS buffer, then centrifuged at 1000g for 5 minutes. Furthermore, we have resuspended the cells in 500µl FACS-buffer. We FACS-sorted CD44+/ALDHbright as CSCs and CD44-/ALDHdim as the non-CSCs population. We have also provided the staining strategy in **Supplementary Table 3.** FACS analysis and processing were performed on the FACS Aria I or III using FACS FlowJo software. Gating strategy is provided in the **Supplementary Fig. 17b**

- ***In vivo* tumorigenesis assay of skin SCC and oral SCC cell lines:**

  To determine the tumorigenic potential of skin SCC cell line (A3886 VC, A3886 Sfrp1 OE) and oral SCC cell lines (ACOSC4 VC, ACOSC4 Sfrp1 OE, ACOSC3 VC, ACOSC3 Sfrp1 OE, and ACOSC16 VC, ACOSC16 Sfrp1 OE), We mixed one million cells from each cell line in 100µl media: matrigel (3:1). We subcutaneously injected the mixture of cells and matrigel into the flank of NOD/SCID mice. The tumor volumes were assessed using vernier calipers every week. Furthermore, we plotted the tumor with respect to time using GraphPad Prism 8.

- ***In vitro* spheroid formation assay:**

  We FACS-sorted 10,000 CSCs and non-CSCs from the skin SCC cell line (A3886, ACSCC1), collected them in media, and centrifuged them at 400g for 15 minutes at 4°C. The cells were resuspended in 1ml serum-free media (Cat no: #05620, Stem Cell Technologies), seeded in ultra-low attachment plates, and incubated at 37°C for 8-10 days. Additionally, we have performed spheroid formation with A3886 VC CSCs and A3886 Sfrp1OE CSCs. We have collected 10,000 FACS-sorted A3886 VC CSCs and A3886 Sfrp1 OE CSCs, resuspended them in 1ml serum-free medium, seeded them in an ultra-low attachment plate, and incubated them at 37°C for 8-10 days. The spheroids were counted manually to compare A3886 VC CSCs and A3886 Sfrp1 OE CSCs. We acquired the images of the spheroid using the Nikon Ti Eclipse microscope. The number of spheroids were plotted in GraphPad Prism 8.

ARTICLE IN PRESS

- ***In vivo* tumorigenesis assay of skin CSCs:**

  To understand the role of Sfrp1 in regulating CSCs, we have isolated 20,000 CSCs from the A3886 VC and A3886 Sfrp1 OE cells using FACS. We mixed the FACS-sorted cells with 75µl DMEM and 25µl Matrigel in a 3:1 ratio and injected the mixture subcutaneously into the flank of NOD/SCID mice. We monitored tumor progression weekly and assessed tumor volumes using a vernier caliper. The mice were sacrificed when tumor volumes reached 20mm in diameter. The tumor volumes were plotted with respect to time using GraphPad Prism 8.

- **Serial transplantation assay of skin CSCs:**

  To understand the self-renewal capacity of CSCs *in vivo*, we have serially transplanted the CSCs subcutaneously in the flank of NOD/SCID mice. We have isolated the 20,000 CSCs from the A3886 skin SCC cell line by FACS. CSCs were 1st transplanted subcutaneously in the flank of NOD/SCID mice after being mixed with the 75µl DMEM and 25µl Matrigel (3:1). Tumors were monitored weekly, tumor volumes were assessed using a vernier caliper, and mice were sacrificed when tumor volumes reached 20mm in diameter. Tumours were harvested, and FACS was performed to isolate CSCs from the tumours and to transplant them into NOD/SCID mice. Similarly, we have performed three consecutive serial transplantations of 20,000 CSCs to show the self-renewal capacity. The tumor volumes were plotted with respect to time using GraphPad Prism 8.

- ***In vivo* metastasis assay:**

  We FACS-isolated CSCs from the A3886 VC and A3886 Sfrp1 OE and collected them in ice-cold DMEM media. The FACS-sorted CSCs were centrifuged at 400g for 15 minutes at 4°C and then resuspended in 100µl of incomplete DMEM medium. We injected the 20,000 CSCs from the A3886 VC and A3886 Sfrp1 OE through the tail vein of NOD/SCID mice. We monitored the injected mice for 30 days. Furthermore, the mice were sacrificed, and we harvested their lungs for analysis to identify metastasis. The number of metastatic colonies was counted and plotted in GraphPad Prism 8 to represent the number of metastases per lung.

- **PET/CT analysis:**

  We investigated the metastasis of A3886 VC, A3886 Sfrp1 OE, ACOSC4 VC, ACOSC4 Sfrp1 OE, ACOSC3 VC, ACOSC3 Sfrp1 OE, ACOSC16, and ACOSC16 Sfrp1 OE cell lines in NOD/SCID mice using PET and CT analysis. We intravenously injected 50-60 µCi (75-100 µl) of 18F FDG via the tail vein and sacrificed the mice 1-hour post-injection. We positioned the mice on the PET scanner bed and conducted a 5-minute scan, with each frame lasting 30 seconds. We analyzed the

ARTICLE IN PRESS

reconstructed images using Visual Eye software (Bioemtech) and delineated the region of interest (ROI) around the tumor to quantify PET activity. Additionally, we performed CT scans on the mice to assess lung metastasis, using a Quantum GX2 scanner (Perkin Elmer) for a 4-minute scan. We analyzed the CT images with Analyze Direct (Analyze 14.0 Software).

- **Clonogenic assay:**

  We seeded 3,000 A3886 VC and A3886 Sfrp1 OE cells to assess colony-forming capacity. The colony-forming capacity was observed for 7-10 days. Furthermore, colonies were fixed using the 4% PFA for 15 minutes. The colonies were washed with 1X PBS twice and stained with 0.05% crystal violet for 45 minutes at room temperature. The crystal violet solution was discarded, followed by two washes of 1X PBS. Colonies were counted and plotted in GraphPad Prism 8.

- **BrdU cell proliferation assay:**

  To study cell proliferation in A3886 VC and A3886 Sfrp1 OE, we serum-starved the cells for 36 hours to synchronise the cell cycle. Furthermore, the complete DMEM medium containing BrdU (10µM) was added and incubated for 10 hours. The cells were fixed with 4% PFA for 20 minutes, followed by 0.3% Triton X treatment for 20 minutes for cell permeabilization. Next, 2N HCl treatment was given for 45 minutes at 37°C. The BrdU +ve cells were stained with anti-BrdU antibodies and detected by an IFA assay. The 50 fields were counted and plotted as % of BrdU +ve cells. The images were acquired using the Zeiss LSM780 confocal microscope. BrdU +ve cells were plotted in GraphPad Prism 8.

- **Cell cycle analysis:**

  We serum-starved A3886 VC and A3886 Sfrp1 OE cells for 36 hours to synchronize the cell cycle, followed by adding a complete medium for 48 hours. The cells were harvested using a 0.25% Trypsin-EDTA solution. The cells were washed with 1X PBS, centrifuged at 1000g for 5 minutes, resuspended in 200 200µl 1X PBS, and fixed with 70% ethanol. The cells were centrifuged at 1000g for 10 minutes and resuspended in the 500µl 1X PBS. PI (1mg/ml) and RNase A (1mg/ml) (Cat no: 556746, Sigma) were added and incubated at 37°C for 20 minutes. The cells were acquired for cell cycle on the Attune Nxt (Thermofisher) machine and analyzed using ModFit software. The percentages of cells in the different phases of the cell cycle were plotted using GraphPad Prism 8.

ARTICLE IN PRESS

- **TOP/FOP Flash assay:**

  The transcriptional activity of β-*CATENIN* in A3886 VC and A3886 shJNK (JNK knockdown) cells was assessed using the TOP/FOP reporter system. We used the M50 Super 8× TOPflash reporter plasmid, which contains TCF/LEF binding sites attached to the luciferase reporter (Gift from Dr. Neelam Shirshat, Addgene plasmid Cat no:#12456). The plasmid pCS-CG, which contains the gene for enhanced green fluorescent protein (EGFP) (Addgene plasmid Cat. no. #12154), was used to evaluate transfection efficiency. A3886 VC and A3886 shJNK cells were transfected with a vector expressing Renilla luciferase (Promega) and a firefly luciferase reporter plasmid TOP Flash, where β-*CATENIN* binds, or the negative control FOP Flash. We performed the transfection using Lipofectamine LTX in 1 x $10^{\wedge 5}$ cells. After 24 hours of incubation, we collected the cells and analyzed them to determine the levels of firefly and Renilla luciferase activity. The luciferase activity was measured in the total protein lysate of the transfected cells and adjusted based on the Renilla luciferase fluorescence using the Cytation 5 Hybrid Multimode Reader (Agilent Technologies) as per the manufacturer's recommendation.

- **Immunofluorescence (IFA) assay of tumor and cultured cell lines:**

  We embedded the tumor tissues in OCT (Cat no: 14020108926, Leica) and cut 5-7µm sections on slides. The sections were fixed using 4% paraformaldehyde (4% PFA) or chilled acetone for 20 minutes, then rinsed with 1X PBS three times, each for 5 minutes. In the case of the cultured or FACS-sorted cells, the cells were seeded on the coverslips and fixed with 4% PFA for 15 minutes. We treated the tissue sections with 0.1% or 0.3% Triton-X for 15 minutes at room temperature for permeabilization. Furthermore, blocking was performed using 5% normal goat serum (NGS) for 1 hour at room temperature. Primary antibodies were incubated overnight at 4°C. The following day, sections were rinsed with the 1X PBS wash three times for 5 minutes each to remove the primary antibody, and the secondary antibody was incubated for 1 hour at room temperature. Hoechst (1mM) was used for nuclear staining for 5 minutes, and slides were mounted using Vectashield antifade (Cat no: H-1000; Vector Lab). The images were acquired using the Zeiss LSM780 confocal microscope.

- **Immunohistochemistry (IHC) assay:**

  We performed IHC on paraffin-embedded tumour sections from advanced-stage skin and oral SCC patient samples. The tumor sections were heated, deparaffinized at 65°C, and rehydrated. Antigen unmasking was carried out with Tris-EDTA buffer (600mg Tris and 180mg EDTA for 500ml and

ARTICLE IN PRESS

250µl Tween-20) (pH 9.0) for cytoplasmic and nuclear proteins (EZH2, c-JUN, and SFRP1) sodium citrate buffer (2.57g Sodium citrate for 500 ml and 250µl Tween-20) (pH 6.0) for membrane protein (WNT7B) in the microwave at 50%-70% power for 10-12 minutes. Furthermore, we blocked endogenous peroxidase activity at room temperature using 5% H_2O_2 in methanol for 10 minutes. We performed blocking with 5% normal horse serum (NHS) at room temperature for 1 hour. We added the primary antibody, prepared in the 5% blocking buffer, to the sections and incubated them at 4°C overnight. The following day, sections were washed at room temperature with 0.2% PBST (PBS with Triton-X) 3 times for 5 minutes. The universal biotinylated secondary antibody was added to the sections for 1 hour, followed by the treatment of freshly prepared avidin-biotin reagent (ABC reagent) (Cat no: PK6200, Vector lab) for 1 hour at room temperature. Diaminobenzidine (DAB) was used as a substrate to detect HRP activity. The counterstaining was performed with hematoxylin for 30 seconds, and Dibutylphthalate Polystyrene Xylene (DPX) mountant (Cat no: 100579, Merck) was used to mount the slides. The IHC images were acquired using the Leica Microsystems CMS fluorescence microscope (Leica). IHC slides were scored by molecular pathologists. IHC score was represented by the H-Score (0-300), based on the intensity of staining. For more details, refer to the section Image acquisition and Statistical analysis.

- **RNA isolation and Real-Time PCR:**

We cultured the cell lines in 60mm plates until 80% confluency for RNA extraction. The complete medium was removed, and the cells were washed three times with chilled 1X PBS. Next, cells were lysed using 1ml TRIZOL (Cat no:T3934, Merck) and the lysate was collected into a 1.5ml centrifuge tube. In the case of the tumor tissue, we have minced the tissue using liquid nitrogen (LN2). The fine powder of tumor tissue was collected in the 1.5ml centrifuge tube, and 1ml TRIZOL was added. Furthermore, the samples were frozen at -80ºC for future use. The samples were thawed on ice, and 250µl of chloroform was added to the tube. Tubes were shaken vigorously and kept undisturbed for 10 minutes at RT. The samples were centrifuged at 12000g for 15 minutes at 4°C, and the aqueous upper layer (40%) was carefully pipetted out without disturbing the interphase and transferred into a fresh 1.5ml tube. We have added 500µl of isopropanol and mixed gently by inverting the tubes several times. Tubes were then left undisturbed for 10 minutes at RT. Furthermore, the samples were centrifuged at 12000g for 10 minutes at 4°C. The supernatant was discarded, and the pellet was resuspended in 1ml 75% ethanol. Samples were then centrifuged at 7600g for 10min. The supernatant was discarded, and the pellet was air-dried. RNA was dissolved

ARTICLE IN PRESS

in the 20µl nuclease-free water. The quality and concentration of RNA were analyzed using the Nano-Drop Spectrophotometer (Thermo Scientific).

RNA isolation from the FACS-sorted CSCs was performed using the picopure RNA isolation kit as per the manufacturer's recommendation (Cat no: KIT0204, Applied Biosystems). The RNA quality and integrity were assessed using the high-sensitivity RNA ScreenTape on the 4200 Tapestation system (Agilent Technologies).

The first strand of cDNA was synthesized using the Primescript RT reagent kit (Cat no: RR037A, Takara) in 20µl of the final volume. A total of 1µg of RNA was converted into cDNA. We have used a 10ng/µl final concentration of cDNA for Real-Time PCR analysis. Real-Time PCR assay was performed using 5 ng of cDNA as a template with TB Green Premix (Cat. no. RR820A, Takara) on the QuantStudio V (Applied Biosystems). β-Actin, GAPDH, and RPS13 genes were used as internal controls for normalization. Each gene's fold change was calculated using the standard $2^{-\Delta\Delta Ct}$ method. Real- PCR primer details are in the **Supplementary Table 4.**

- **Protein isolation from cultured cell lines, SCC tumor, and FACS-sorted CSCs:**

We cultured the primary keratinocytes until they reached 80-85% confluency in 100mm Petri plates. We washed the cells twice with ice-cold 1X PBS for 5 minutes. We added 400µl of RIPA buffer (Cat no: R2078, Sigma) and 1X of protease/phosphatase inhibitors (Roche) and kept the mixture on ice for 15 minutes. We scraped the cells using a cell scraper and centrifuged the lysate at 12,000g for 15 minutes at 4°C. The supernatant was transferred to fresh tubes and stored at -80°C. The protein estimation was performed using the Bradford assay as per the manufacturer's recommendation (Cat no: ML106, Himedia).

Furthermore, a small tumor was minced in liquid nitrogen to isolate protein from the SCC tumors. The resulting fine powder was collected, and 350µl of RIPA buffer containing the inhibitor (Phosphatase & Protease) cocktail was added. The sample was snap-frozen and stored at -80°C. The following day, the sample was allowed to thaw on ice and vortexed vigorously at 10-minute intervals. Once the sample was thawed completely, the lysate was centrifuged at 12,000g for 30 minutes at 4°C. The supernatant was transferred to fresh tubes and stored at -80°C. The protein estimation was performed using the Bradford assay as per the manufacturer's recommendation (Cat no: ML106, Himedia). Furthermore, FACS-sorted CSCs and non-CSCs were collected in complete DMEM to isolate the protein from the FACS-sorted CSCs. The cells were centrifuged at 1000g for 15 minutes at 4°C. The cell pellet was washed with 1X PBS for 5 minutes, resuspended in 150µl of

ARTICLE IN PRESS

RIPA buffer containing the inhibitor cocktail, and kept on ice for 30 minutes. The lysate was centrifuged at 12,000g for 30 minutes at 4°C. The supernatant was collected and stored at -80°C. The protein estimation was performed using the Bradford assay as per the manufacturer's recommendation (Cat no: ML106, Himedia).

- **ChIP-qPCR assays:**

A3886 VC, A3886 Sfrp1 OE, ACOSC4 VC, ACOSC4 Sfrp1 OE, ACOSC3 VC, ACOSC3 Sfrp1 OE, ACOSC16, ACOSC16 Sfrp1 OE cell lines were used to assess the binding of c-*JUN* on the *SOX2* promoter region. A3886 VC, A3886 + DAC, ACOSC4 VC, ACOSC4 + DAC, ACOSC3, and ACOSC3 + DAC cells were used to assess the binding of H3K27me3 on the *SFRP1*promoter region, H3K27ac on the *SFRP1* promoter region, 5 methyl Cytosine (5-mc) on the *SFRP1*promoter region, *SOX2* binding on the *HIF1α* promoter region, and *HIF1α* binding on the *SLC2A2*, *HK2*, and *LDHA* promoter region.

One million cells were cross-linked by adding 0.75% formaldehyde into the media and gently spinning the mixture at room temperature for 10 minutes. 125mM Glycine was used to quench the cross-linking of the cells, which were scraped and centrifuged at 1000g for 5 minutes at 4°C. Furthermore, the pellets were resuspended in the ChIP lysis buffer (50mM HEPES-KOH, pH 7.5, 140mM NaCl, 1mM EDTA, pH 8 1% Triton X-100, 0.1% Sodium Deoxycholate, 0.1% SDS) and sonicated using a bioruptor (Diagenode) to produce chromatin fragments of 200-1000 bp in size.

To understand the enrichment of histone marks and DNA methylation pattern on the Sfrp1 promoter, we have also performed the Mono-nucleosomal ChIP using the MNase (Cat no: M0247S, NEB) treatment on the chromatin.

4µg of c-JUN (Cat no: #9165, CST), 5µg of H3K27me3 (Cat no: #9733, CST), 4µg of H3K27ac (Cat no: #8173, CST), 5µg of 5-methylcytosine (5-mc), 4µg of Sox2 (Cat no: ab92494, abcam), 4µg of HIF1α (Cat no: SAB2702132, Sigma) were incubated with 10-15µg of chromatin overnight at 4°C, followed by incubation with Sepharose protein G beads (Cytiva) for 4 hours at 4°C. Furthermore, after multiple washing steps (Low salt buffer) (0.1% SDS 1% Triton X-100, 2mM EDTA, 20mM Tris-HCl, pH 8.0, 150mM NaCl), DNA was eluted by reverse crosslinking overnight at 65 °C. DNA was purified using by PCR purification kit. Furthermore, for Real-Time PCR, 2µl of enriched DNA and 1µM of primers and TB green premix were subjected to 40 cycles of PCR using Quant Studio V (Applied Biosystems). The percentage input method was used to calculate the enrichment of the genomic region. 1% chromatin was used as input. We have used bead control

ARTICLE IN PRESS

and IgG control to show the background binding of chromatin. ChIP-qPCR primer details are in **Supplementary Table 5**.

- **Western blot analysis:**

The SDS-PAGE gel was prepared using 30% bis-acrylamide. We have used an 8-15% resolving gel based on protein molecular weight. Furthermore, samples were mixed with 6X loading dye and incubated at 95ºC for 5 minutes to denature. The 40-60 µg range of protein was loaded in each lane and resolved by electrophoresis. The gel was run at 60V for stacking and 80V for resolving at RT. Furthermore, the protein was transferred to the 0.45µm PVDF membrane at 180mA for 3 hours at 4°C (Cat no: IPVH00010, Millipore). The membrane was blocked using the 5% BSA or 5% non-fat milk powder in 1X TBST (6.2g Tris, 8.76g NaCl, and 1ml Tween-20 for 1 liter) for 1 hour at room temperature. The membrane was kept in the primary antibody overnight at 4°C. The following day, the membrane was washed with 1X TBST three times for 15 minutes each to remove the residual primary antibody. It was incubated at room temperature with HRP-conjugated anti-rabbit or anti-mouse secondary antibody for 1 hour. The ECL prime (Cat no: RPN2232, Cytiva) substrate was used to develop the membrane on the Chemidoc (Bio-Rad). We have used H3 as an internal control for epigenetic modifiers and β-Tubulin as an internal control for the rest of the proteins. The densitometric analysis of the western blot was performed with respect to the internal control on the Image Lab 6.0 software (Bio-Rad). Antibody details are provided in the **Supplementary Table 6.**

- **Treatment with the pharmacological drug DAC and RAC1i (NSC23766):**

DAC is 5-aza-2-deoxycytidine, a cytosine analog, which inhibits methyltransferase activity. We have dissolved the DAC in autoclaved Milli-Q water and used it for cell culture and the *in vivo* tumorigenesis experiment. To impede hypermethylation of the Sfrp1 promoter, we treated the A3886, ACOSC4, and ACOSC3 cell lines with 4.2µM DAC for 72 hours. The cells were used for the ChIP-qPCR experiment. We have injected one million cells of A3886, A3886 Sfrp1 OE, ACOSC4, ACOSC4 Sfrp1 OE, ACOSC3, and ACOSC3 Sfrp1 OE subcutaneously into the flank of NOD/SCID mice. Furthermore, the tumor development was monitored weekly, and tumor volume was assessed using a vernier caliper. The DAC (0.8mg/kg body weight) was injected intraperitoneally twice a week into mice, while the RAC1i/NSC23766 (Rac1 inhibitor) (Cat no: HY-15723A, MedChemExpress) (0.5mg/kg body weight) was injected intraperitoneally.[69,70]. Mice were sacrificed when the tumor in the control group reached 20mm. Tumors were harvested from the mice and used for the Real-time PCR and western blot.

ARTICLE IN PRESS

- **Enzyme/substrate assay:**

  We have checked the Pyruvate (Cat no: MAK332, Sigma), Lactate (Cat no: MAK570, Sigma), Acetyl Co-A levels (Cat no: MAK039, Sigma), and Lactate dehydrogenase (LDH) activity was measured as per the manufacturer's recommendation (Cat no: MAK066, Sigma). We FACS-sorted 0.1million skin SCC CSCs and non-CSCs in the LDH assay buffer and centrifuged them at 10,000g for 15 minutes at 4°C. NADH was the standard, and five different standard concentrations were used for the standard curve (0 to 12.5nmol/well). Furthermore, the substrate was added to the test samples, and absorbance was taken at 450nm every 5 minutes till 30 minutes (till the final concentration fell within the range of the standard). LDH activity was reported as µmole/min/ml. A3886 VC, A3886 Sfrp1 OE, ACOSC4 VC, ACOSC4 Sfrp1 OE, ACOSC3 VC, ACOSC3 Sfrp1 OE, ACOSC16, ACOSC16 Sfrp1 OE, A3886 + DAC, ACOSC4 + DAC, and ACOSC3 + DAC cells were used to identify the substrate levels of Pyruvate, Lactate, and Acetyl Co-A. We used five different concentrations for the standard curve (0 to 12.5nmol/well). The enzymes were added and incubated at 37°C for 30 minutes. The absorbance was taken at 570nm. Substrate concentration was reported in ng/µl, and the graph was plotted using GraphPad Prism 8.

- **Glycolytic rate assay by Seahorse experiment:**

  We have seeded the skin SCC cell lines (A3886, ACSCC1), HEKa, oral SCC cell lines (ACOSC3, ACOSC4, ACOSC16), and HOK in the Agilent Seahorse XF 24-well Cell Culture Microplate (Cat no: 103723-100, Agilent) prior day before the experiment. We have also hydrated the sensor cartridge in Seahorse XF Calibrant solution at 37 °C in a non-CO2 incubator overnight, a day before the experiment. On the day of the experiment, we washed the cells twice with Seahorse assay medium (Seahorse XF DMEM) (Cat no: 103575-100, Agilent) adjusted to pH 7.4 (1 mM pyruvate, 2 mM glutamine, and 10 mM glucose). We kept the cells in the non-CO2 incubator for 2 hours. We have changed the medium of the cells and added fresh medium before the measurement of the glycolytic rate of the cells. For glycolytic rate measurement, we have injected the Rotenone/Antimycin mixture (0.5µM) (Rotenone Cat no: R8875, Sigma) (Antimycin Cat no: A8674, Sigma) in Port A and 2-deoxy glucose (2DG) (50mM) (Cat no: D8375, Sigma) in Port B. The glycolytic rate was measured on the Seahorse XFe24 Analyzer (Agilent Technologies). Furthermore, we have lysed the cells in each well by adding 100µl of RIPA buffer. We have isolated the protein from each well and calculated to normalize the Seahorse measurements.

ARTICLE IN PRESS

- **TCGA analysis:**

  Xena is a web-based database available at https://xenabrowser.net/heatmap/. It is a useful tool for viewing and evaluating functional genomic data in the context of clinical research. This platform is built in JavaScript. For this study, we used UCSC Xena to generate a correlation heatmap of mRNA expression for the *EZH2*, *SFRP1*, *WNT7B*, and c-*JUN* genes. The analysis was performed on patients from the TCGA HNSCC datasets. We evaluated the expression of EZH2, SFRP1, WNT7B, and c-JUN and the prognosis of patients with HNSCC, using OS as the endpoint. OS analysis was represented by using the Kaplan-Meier plot, and a Cox-regression p-value of less than 0.05 was considered.

- **RNA sequencing library preparation and data analysis:**

  We have performed RNA sequencing analysis on the different combinations described in **Supplementary Table 7**. We used the 5ng of extracted RNA to prepare the 300bp cDNA libraries using the SMARTer Stranded Total RNA-seq kit v3- pico input mammalian from Takara Bio Inc., per the manufacturer's recommendation (Cat. No. 634485, Takara Bio). We sequenced the Total RNA at 150bp (paired-end) using the Illumina NovaSeq 6000 platform. 60 million paired-end reads were generated per sample. Furthermore, QC of generated reads was carried out using FastQC version 0.11.9 [71], Pre-processing of Raw FASTQ files was done using fastp version 0.23.4[72]. The reads were aligned against the human genome assembly (GrCh38) (available on the Ensembl database) using HISAT2 version 2.2.1[73]. We converted the SAM file output to a BAM format, and the BAM files were sorted by name using SAMtools version 1.6[74]. The quality of the alignment was identified using Qualimap version 2.2.2[75]. The counting of the mapped reads was performed using feature Counts version 2.0.6[76]. Differential expression analysis was determined by the count data with the DESeq2 package version 1.42.0[77]. The PCA of the DESeq2 analysis was done using the pca Explorer package version 2.28.0[78]. Volcano plot of the DEGs was plotted using the Enhanced Volcano package version 1.20.0[79]. The heatmaps for the DEGs with padj>0.05, top 100 DEGs, and top 200 DEGs were generated using the Complex Heatmap package version 2.18.0[80]. The customized heat maps of genes associated with epigenetic and metabolic signatures were generated using the pheatmap package version 1.0.12[81]. Gene Set Enrichment Analysis (GSEA) for A3886 CSCs Vs. non-CSCs and patient sample CSCs vs. non-CSCs were performed using GSEA v4.4.3 software hosted by the Broad Institute[82]. The gene sets used for the analysis were obtained

ARTICLE IN PRESS

from the molecular signatures database (MSigDB)[83]. We have deposited all the RNA sequencing data under accession code PRJEB101821 in the EMBL-EBI European Nucleotide Archive (ENA).

- **Statistical analysis:**

We have performed two-tailed Student t-tests or multiple-t-test followed by Holm-Bonferroni correction, for densitometric analysis of Western blot, Real-Time PCR, ChIP-qPCR, Enzyme/substrate analysis, and identification of the number of keratin pearls in mice; two-way ANOVA followed by Dunnett's test were used to assess the *in vivo* tumorigenesis experiments, and Mann-Whitney test was used to assess the overlap coefficient of markers (KERATIN-14 & VIMENTIN) (E-CADHERIN & β-CATENIN), number of lung metastases using GraphPad Prism 8.

The densitometric analysis of the western blot was performed on the Image Lab 6.0 software (Bio-Rad). IHC images were acquired using the Leica Microsystems CMS fluorescence microscope (Leica). Luciferase fluorescence was measured using the Cytation 5 Hybrid Multimode Reader (BioTek). Cell cycle was performed on the Attune Nxt (Thermofisher) machine and analyzed using ModFit software. FACS-sorted cells were acquired using the FACS ARIA-I or III (BD Biosciences). FACS data were analyzed using FlowJo software 10.0. PET/CT images were analyzed using Analyze Direct 14.0. The spheroid images were taken on the Nikon Eclipse Ti microscope. Spheroid images were analyzed using the ImageJ software 6.0. Glycolytic rate was measured using the Seahorse xFe24 analyzer. Glyolytic rate was analyzed by using Wave Software 2.6.1. All the IFA images were analyzed using the Zen black software (Zen 3.0). Furthermore, we analyzed the colocalization and overlap coefficient between K14, VIMENTIN, E-CADHERIN, and β-CATENIN using Zen black software.

The two independent pathologists (PG, SR & BR) scored the IHC of markers EZH2, SFRP1, WNT7B, and c-JUN. IHC was scored based on the intensity and represented by an H-score (0-300). The H-score was plotted using GraphPad Prism 8, and the Mann-Whitney test was performed to analyze the data. We used SPSS software to analyze survival analysis (Kaplan-Meier) and the normalization of patient data determined by the Spearman Rho test and the Pearson coefficient test. OS was determined by comparing the specific markers' Kaplan-Meier (KM) survival curves. These markers were considered by multivariate analysis using Cox regression if they were shown to be significant by KM analysis. We have used the Mann-Whitney U test for the quantitative comparison of H-Scores between skin and oral SCC. We have used biological replicates for all the experiments

ARTICLE IN PRESS

and analyzed all the statistical data. A p-value of 0.05 or less was considered statistically significant for the entire study.

Data availability statement

We have deposited all the RNA sequencing data under accession code PRJEB101821 in the EMBL-EBI European Nucleotide Archive (ENA) and made it publicly available. We have provided FACS gating strategies in **Supplementary Fig.16 & 17**. We have provided FACS staining strategies in the Supplementary information (**Supplementary Table 1-3**). We have provided primer and antibody details in the Supplementary information (**Supplementary Table 4-6**). We have provided the statistical analysis of each figure as a Source Data file. We have also provided uncropped blots in the Source Data file.

ARTICLE IN PRESS

ARTICLE IN PRESS

5. References

1. Hoadley, K. A. *et al.* Multiplatform analysis of 12 cancer types reveals molecular classification within and across tissues of origin. *Cell* **158**, (2014).

2. Allis, C. D. & Jenuwein, T. The molecular hallmarks of epigenetic control. *Nature Reviews Genetics* vol. 17 Preprint at https://doi.org/10.1038/nrg.2016.59 (2016).

3. Greenberg, M. V. C. & Bourc'his, D. The diverse roles of DNA methylation in mammalian development and disease. *Nature Reviews Molecular Cell Biology* vol. 20 Preprint at https://doi.org/10.1038/s41580-019-0159-6 (2019).

4. Liu, W. *et al.* Histone-methyltransferase KMT2D deficiency impairs the Fanconi anemia/BRCA pathway upon glycolytic inhibition in squamous cell carcinoma. *Nat. Commun.* **15**, (2024).

5. Yang, F., Zeng, Q., Yu, G., Li, S. & Wang, C. Y. Wnt/β-catenin signaling inhibits death receptor-mediated apoptosis and promotes invasive growth of HNSCC. *Cell. Signal.* **18**, (2006).

6. Geyer, F. C. *et al.* B-Catenin pathway activation in breast cancer is associated with triple-negative phenotype but not with CTNNB1 mutation. *Modern Pathology* **24**, (2011).

7. Nager, M. *et al.* β -Catenin Signalling in Glioblastoma Multiforme and Glioma-Initiating Cells . *Chemother. Res. Pract.* **2012**, (2012).

8. Sherwood, V. & Leigh, I. M. WNT Signaling in Cutaneous Squamous Cell Carcinoma: A Future Treatment Strategy? *Journal of Investigative Dermatology* vol. 136 Preprint at https://doi.org/10.1016/j.jid.2016.05.108 (2016).

9. Liu, S. *et al.* High Vimentin Expression Associated with Lymph Node Metastasis and Predicated a Poor Prognosis in Oral Squamous Cell Carcinoma. *Sci. Rep.* **6**, (2016).

10. Liu, L. J. *et al.* Aberrant regulation of WNT signaling in hepatocellular carcinoma. *World Journal of Gastroenterology* vol. 22 Preprint at https://doi.org/10.3748/wjg.v22.i33.7486 (2016).

11. Liu, C., Takada, K. & Zhu, D. Targeting Wnt/β-Catenin Pathway for Drug Therapy. *Medicine in Drug Discovery* vol. 8 Preprint at https://doi.org/10.1016/j.medidd.2020.100066 (2020).

12. Satoh, W., Gotoh, T., Tsunematsu, Y., Aizawa, S. & Shimon, A. Sfrp 1 and Sfrp2 regulate anteroposterior axis elongation and somite segmentation during mouse embryogenesis. *Development* **133**, (2006).

13. Renström, J. *et al.* Secreted Frizzled-Related Protein 1 Extrinsically Regulates Cycling Activity and Maintenance of Hematopoietic Stem Cells. *Cell Stem Cell* **5**, 157–167 (2009).

ARTICLE IN PRESS

14. Sunkara, R. R., Mehta, D., Sarate, R. M. & Waghmare, S. K. BMP-AKT-GSK3β Signaling Restores Hair Follicle Stem Cells Decrease Associated with Loss of Sfrp1. *Stem Cells* **40**, (2022).

15. Kierulf-Vieira, K. S. *et al.* Wnt inhibition is dysregulated in gliomas and its re-establishment inhibits proliferation and tumor sphere formation. *Exp. Cell Res.* **340**, (2016).

16. Chang, L. *et al.* Expression and prognostic value of SFRP1 and β-catenin in patients with Glioblastoma. *Oncol. Lett.* **11**, (2016).

17. Kong, L. Y., Xue, M., Zhang, Q. C. & Su, C. F. In vivo and in vitro effects of microRNA-27a on proliferation, migration and invasion of breast cancer cells through targeting of SFRP1 gene via Wnt/β-catenin signaling pathway. *Oncotarget* **8**, (2017).

18. Wu, F., Li, J., Guo, N., Wang, X. H. & Liao, Y. Q. MiRNA-27a promotes the proliferation and invasion of human gastric cancer MGC803 cells by targeting SFRP1 via Wnt/β-catenin signaling pathway. *Am. J. Cancer Res.* **7**, (2017).

19. Sunkara, R. R. *et al.* SFRP1 in Skin Tumor Initiation and Cancer Stem Cell Regulation with Potential Implications in Epithelial Cancers. *Stem Cell Reports* **14**, 271–284 (2020).

20. Song, J. *et al.* A protein interaction between β-catenin and Dnmt1 regulates Wnt signaling and DNA methylation in colorectal cancer cells. *Molecular Cancer Research* **13**, (2015).

21. Lei, A. *et al.* EZH2 regulates protein stability via recruiting USP7 to mediate neuronal gene expression in cancer cells. *Front. Genet.* **10**, (2019).

22. Liu, W. *et al.* Histone-methyltransferase KMT2D deficiency impairs the Fanconi anemia/BRCA pathway upon glycolytic inhibition in squamous cell carcinoma. *Nat. Commun.* **15**, (2024).

23. Cairns, R. A., Harris, I. S. & Mak, T. W. Regulation of cancer cell metabolism. *Nature Reviews Cancer* vol. 11 85–95 Preprint at https://doi.org/10.1038/nrc2981 (2011).

24. Choi, J. E. *et al.* A unique subset of glycolytic tumour-propagating cells drives squamous cell carcinoma. *Nat. Metab.* **3**, 182–195 (2021).

25. Pate, K. T. *et al.* Wnt signaling directs a metabolic program of glycolysis and angiogenesis in colon cancer. *EMBO J.* **33**, (2014).

26. Pate, K. T. *et al.* Wnt signaling directs a metabolic program of glycolysis and angiogenesis in colon cancer. *EMBO J.* **33**, 1454–1473 (2014).

27. Nakagawa, S. *et al.* Wnt/β-catenin signaling regulates amino acid metabolism through the suppression of CEBPA and FOXA1 in liver cancer cells. *Commun. Biol.* **7**, (2024).

28. Nie, X. *et al.* LRP5 Promotes Gastric Cancer via Activating Canonical Wnt/β-Catenin and Glycolysis Pathways. *American Journal of Pathology* **192**, 503–517 (2022).

ARTICLE IN PRESS

ARTICLE IN PRESS

29. Lee, M. H., Koria, P., Qu, J. & Andreadis, S. T. JNK phosphorylates β-catenin and regulates adherens junctions. *FASEB Journal* **23**, (2009).

30. Gawas, N. P., Navarange, S. S., Chovatiya, G. L., Chaturvedi, P. & Waghmare, S. K. Establishment and characterization of novel human oral squamous cell carcinoma cell lines from advanced-stage tumors of buccal mucosa. *Oncol. Rep.* **41**, (2019).

31. DiNardo, C. D. *et al.* Venetoclax combined with decitabine or azacitidine in treatment-naive, elderly patients with acute myeloid leukemia. *Blood* **133**, (2019).

32. Santini, V., Lübbert, M., Wierzbowska, A. & Ossenkoppele, G. J. The Clinical Value of Decitabine Monotherapy in Patients with Acute Myeloid Leukemia. *Advances in Therapy* vol. 39 Preprint at https://doi.org/10.1007/s12325-021-01948-8 (2022).

33. Zhou, M. *et al.* H3K27me3 Inactivates SFRP1 to Promote Cell Proliferation via Wnt/β-Catenin Signaling Pathway in Esophageal Squamous Cell Carcinoma. *Dig. Dis. Sci.* **68**, (2023).

34. Jiang, X. *et al.* DACT3 Is an Epigenetic Regulator of Wnt/β-Catenin Signaling in Colorectal Cancer and Is a Therapeutic Target of Histone Modifications. *Cancer Cell* **13**, 529–541 (2008).

35. Song, Y. *et al.* The Wnt/β-catenin and PI3K/Akt signaling pathways promote EMT in gastric cancer by epigenetic regulation via H3 lysine 27 acetylation. *Tumor Biology* **39**, 1–10 (2017).

36. Wang, Z., Li, R., He, Y. & Huang, S. Effects of secreted frizzled-related protein 1 on proliferation, migration, invasion, and apoptosis of colorectal cancer cells. *Cancer Cell Int.* **18**, (2018).

37. Zhang, H., Sun, D., Qiu, J. & Yao, L. SFRP1 inhibited the epithelial ovarian cancer through inhibiting wnt/β-catenin signaling. *Acta Biochim. Pol.* **66**, (2019).

38. Lin, H. *et al.* Secreted frizzled-related protein 1 overexpression in gastric cancer: Relationship with radiological findings of dual-energy spectral CT and PET-CT. *Sci. Rep.* **7**, (2017).

39. Losada-García, A. *et al.* SFRP1 induces a stem cell phenotype in prostate cancer cells. *Front. Cell Dev. Biol.* **11**, (2023).

40. Rosso, S. B., Sussman, D., Wynshaw-Boris, A. & Salinas, P. C. Wnt signaling through Dishevelled, Rac and JNK regulates dendritic development. *Nat. Neurosci.* **8**, 34–42 (2005).

41. Lv, H. *et al.* The WNT7B protein promotes the migration and differentiation of human dental pulp cells partly through WNT/beta-catenin and c-Jun N-terminal kinase signalling pathways. *Arch. Oral Biol.* **87**, (2018).

42. Zheng, D. *et al.* Role of WNT7B-induced noncanonical pathway in advanced prostate cancer. *Molecular Cancer Research* **11**, (2013).

ARTICLE IN PRESS

43. Yang, W. *et al.* Epigenetic silencing of JAM3 promotes esophageal cancer development by activating Wnt signaling. *Clin. Epigenetics* **14**, (2022).

44. Pagin, M. *et al.* Sox2 controls neural stem cell self-renewal through a Fos-centered gene regulatory network. *Stem Cells* **39**, (2021).

45. Apostolou, P. *et al.* AP-1 Gene Expression Levels May Be Correlated with Changes in Gene Expression of Some Stemness Factors in Colon Carcinomas. *J. Signal Transduct.* **2013**, (2013).

46. Boumahdi, S. *et al.* SOX2 controls tumour initiation and cancer stem-cell functions in squamous-cell carcinoma. *Nature* **511**, 246–250 (2014).

47. Pastushenko, I. *et al.* Identification of the tumour transition states occurring during EMT. *Nature* **556**, (2018).

48. Pastushenko, I. *et al.* Fat1 deletion promotes hybrid EMT state, tumour stemness and metastasis. *Nature* **589**, (2021).

49. Pastushenko, I. & Blanpain, C. EMT Transition States during Tumor Progression and Metastasis. *Trends in Cell Biology* vol. 29 Preprint at https://doi.org/10.1016/j.tcb.2018.12.001 (2019).

50. Quan, Q. *et al.* Cancer stem-like cells with hybrid epithelial/mesenchymal phenotype leading the collective invasion. *Cancer Sci.* **111**, (2020).

51. Wolf, A., Agnihotri, S., Munoz, D. & Guha, A. Developmental profile and regulation of the glycolytic enzyme hexokinase 2 in normal brain and glioblastoma multiforme. *Neurobiol. Dis.* **44**, (2011).

52. Wan, W. *et al.* Histone demethylase JMJD1A promotes urinary bladder cancer progression by enhancing glycolysis through coactivation of hypoxia inducible factor 1α. *Oncogene* **36**, (2017).

53. Tran, T. Q. *et al.* α-Ketoglutarate attenuates Wnt signaling and drives differentiation in colorectal cancer. *Nat. Cancer* **1**, 345–358 (2020).

54. Yamagishi, M. *et al.* Mechanisms of action and resistance in histone methylation-targeted therapy. *Nature* **627**, (2024).

55. Momparler, R. L., Côté, S., Momparler, L. F. & Idaghdour, Y. Inhibition of DNA and histone methylation by 5-Aza-2'-deoxycytidine (decitabine) and 3-deazaneplanocin-A on antineoplastic action and gene expression in myeloid leukemic cells. *Front. Oncol.* **7**, (2017).

56. Viet, C. T. *et al.* Decitabine rescues cisplatin resistance in head and neck squamous cell carcinoma e112880. *PLoS One* **9**, (2014).

57. Sun, J. *et al.* RAC1 plays an essential role in estrogen receptor alpha function in breast cancer cells. *Oncogene* **40**, (2021).

ARTICLE IN PRESS

58. Wu, Y. jun *et al.* Expression and significance of Rac1, Pak1 and Rock1 in gastric carcinoma. *Asia. Pac. J. Clin. Oncol.* **10**, (2014).

59. Gastonguay, A. *et al.* The role of Rac1 in the regulation of NF-kB activity, cell proliferation, and cell migration in non-small cell lung carcinoma. *Cancer Biol. Ther.* **13**, (2012).

60. Ling, Z. *et al.* Targeting CCL2-CCR4 axis suppress cell migration of head and neck squamous cell carcinoma. *Cell Death Dis.* **13**, (2022).

61. Yoshida, T. *et al.* Blockade of Rac1 activity induces G1 cell cycle arrest or apoptosis in breast cancer cells through downregulation of cyclin D1, survivin, and X-linked inhibitor of apoptosis protein. *Mol. Cancer Ther.* **9**, (2010).

62. Liu, J. *et al.* Metabolic enzyme LDHA activates Rac1 GTPase as a noncanonical mechanism to promote cancer. *Nat. Metab.* **4**, (2022).

63. Li, Z. *et al.* Targeting the Rac1 pathway for improved prostate cancer therapy using polymeric nanoparticles to deliver of NSC23766. *Chinese Chemical Letters* **33**, (2022).

64. Abel, E. L., Angel, J. M., Kiguchi, K. & DiGiovanni, J. Multi-stage chemical carcinogenesis in mouse skin: Fundamentals and applications. *Nat. Protoc.* **4**, (2009).

65. Driessens, G., Beck, B., Caauwe, A., Simons, B. D. & Blanpain, C. Defining the mode of tumour growth by clonal analysis. *Nature* **488**, 527–530 (2012).

66. Conway, K., Morgan, D., Phillips, K. K., Yuspa, S. H. & Weissman, B. E. Tumorigenic Suppression of a Human Cutaneous Squamous Cell Carcinoma Cell Line in the Nude Mouse Skin Graft Assay. *Cancer Res.* **52**, (1992).

67. Mehta, D. *et al.* Establishment and molecular characterization of the novel cutaneous squamous cell carcinoma cell line from advanced-stage Indian patient. *Hum. Cell* **38**, (2025).

68. Gawas, N. P., Navarange, S. S., Chovatiya, G. L., Chaturvedi, P. & Waghmare, S. K. Establishment and characterization of novel human oral squamous cell carcinoma cell lines from advanced-stage tumors of buccal mucosa. *Oncol. Rep.* https://doi.org/10.3892/or.2019.7003 (2019) doi:10.3892/or.2019.7003.

69. Tsai, H. C. *et al.* Transient Low Doses of DNA-Demethylating Agents Exert Durable Antitumor Effects on Hematological and Epithelial Tumor Cells. *Cancer Cell* **21**, (2012).

70. Dahn, M. L. *et al.* Decitabine response in breast cancer requires efficient drug processing and is not limited by multidrug resistance. *Mol. Cancer Ther.* **19**, (2020).

71. Andrews, S. & others. FastQC: a quality control tool for high throughput sequence data. 2010. *Https://Www.Bioinformatics.Babraham.Ac.Uk/Projects/Fastqc/* (2019).

72. Chen, S., Zhou, Y., Chen, Y. & Gu, J. Fastp: An ultra-fast all-in-one FASTQ preprocessor. in *Bioinformatics* vol. 34 (2018).

ARTICLE IN PRESS

ARTICLE IN PRESS

73. Kim, D., Paggi, J. M., Park, C., Bennett, C. & Salzberg, S. L. Graph-based genome alignment and genotyping with HISAT2 and HISAT-genotype. *Nat. Biotechnol.* **37**, (2019).

74. Li, H. *et al.* The Sequence Alignment / Map (SAM) Format and SAMtools 1000 Genome Project Data Processing Subgroup. *Bioinformatics* **25**, (2009).

75. García-Alcalde, F. *et al.* Qualimap: Evaluating next-generation sequencing alignment data. *Bioinformatics* **28**, (2012).

76. Liao, Y., Smyth, G. K. & Shi, W. FeatureCounts: An efficient general purpose program for assigning sequence reads to genomic features. *Bioinformatics* **30**, (2014).

77. Love, M. I., Anders, S. & Huber, W. *Differential Analysis of Count Data - the DESeq2 Package*. *Genome Biology* vol. 15 (2014).

78. Marini, F. & Binder, H. PcaExplorer: An R/Bioconductor package for interacting with RNA-seq principal components. *BMC Bioinformatics* **20**, (2019).

79. Blighe K, Rana S & Lewis M. Publication-ready volcano plots with enhanced colouring and labeling. *Bioconductor* (2022).

80. Gu, Z., Eils, R. & Schlesner, M. Complex heatmaps reveal patterns and correlations in multidimensional genomic data. *Bioinformatics* **32**, (2016).

81. Kolde, R. Package 'pheatmap': Pretty heatmaps. *R package* (2022).

82. Subramanian, A. *et al.* Gene set enrichment analysis: A knowledge-based approach for interpreting genome-wide expression profiles. *Proc. Natl. Acad. Sci. U. S. A.* **102**, (2005).

83. Liberzon, A. *et al.* Molecular signatures database (MSigDB) 3.0. *Bioinformatics* **27**, (2011).

ARTICLE IN PRESS

ARTICLE IN PRESS

Acknowledgements:

This work was supported by the Advanced Centre for Treatment Research and Education in Cancer, Department of Atomic Energy, ACTREC annual fund (grant no. DAE-ACTREC 4598, 4479 to S.K.W). We thank the Tata Memorial Centre Research Administration Council for providing financial support (TRAC-3542, IEC#188 to S.K.W). D.M. and A.P. are supported by the ACTREC fellowship.

We thank Dr. Akihiko Shimono, Japan, for providing the Sfrp1 knockout mice. We thank Dr. Colin Jamora, Shiv Nadar University, Delhi, for providing the A3886 human skin SCC cell line. We thank Dr. Neelam Shirshat, ACTREC-TMC, Navi Mumbai, for providing Tet-pLKO-puro and TOP/FOP FLSH plasmids. We thank the ACTREC Animal House, small animal imaging facility, flow cytometry, genomic facility, digital imaging, and electron microscopy facilities. We thank the Tumor Tissue Repository, Tata Memorial Hospital, Tata Memorial Centre-ACTREC Biorepository, and Department of Pathology for providing tumor tissues. We thank Dr. Sanjay Gupta (Epigenetics and Chromatin Biology Group, ACTREC-TMC, Navi Mumbai) for his valuable insights and discussion on epigenetic aspects. We thank Dr. Avik Chakraborty (Radiation Medicine Centre, BARC, TMH, Mumbai) for allowing us to use the Seahorse xFE24 instrument for understanding glycolysis rate. We thank Mr. Jitendra Gawde (Department of Statistics, ACTREC-TMC, Navi Mumbai) for providing the OS analysis of skin and oral SCCs patients and quantitative comparison of IHC H-scores and gene signatures in skin and oral SCCs patients. The graphical abstract was prepared using Biorender (Created with https://www.biorender.com/). We have also provided the licensed copy of Biorender (https://biorender.com/j34ubni)

Author contributions

S.K.W. conceived and designed the project and analyzed and interpreted the data. D.M. has performed all *in vivo* experiments, Flow cytometry, IFA, Western blot, ChIP-qPCR, and IHC of skin and oral patient samples, normal skin and oral mucosa (adjacent margin), and TCGA analysis. A.P. performed all RNA sequencing analysis and Gene Set Enrichment Analysis (GSEA). P.N. has provided the skin SCC tumor and normal skin (adjacent margin) samples. P.C. has provided oral SCC tumor samples, S.R. has provided the normal oral mucosa (adjacent margin) samples, and P.G., S.R., and B.R. have scored the IHC slides of skin and oral SCCs. P.C. and B.M. have

ARTICLE IN PRESS

performed the *in vivo* metastasis, PET imaging, and data analysis. S.K.W. and D.M. analyzed all the data. S.K.W. and D.M. wrote the manuscript.

Competing interests

The authors declare no competing interests.

ARTICLE IN PRESS

ARTICLE IN PRESS

5. Figure legends:

Figure 1: Enrichment of non-canonical Wnt signaling and glycolysis in skin and oral SCC patients

a) Representative image of flow cytometry analysis between CSCs and non-CSCs isolated from the advanced-stage skin SCC patient biopsy and normal skin tissue (adjacent margin)

b) Graphical representation of CSCs and non-CSCs isolated from the advanced-stage skin SCC patient biopsy (n=6) and normal skin tissue (adjacent margin) (n=6), mean ± SEM, two-tailed Mann-Whitney U test

c) Validation of CSCs and non-CSCs isolated from the advanced-stage skin SCC patient biopsy and normal skin tissue (adjacent margin) by Real-Time PCR, n=3 biological replicates, mean ± SEM, two-tailed multiple t-test followed by Holm-Bonferroni correction

d) Representative image of IHC analysis of SFRP1, WNT7B, and c-JUN in the retrospectively collected advanced-stage skin SCC patient samples and normal skin samples (adjacent margin)

e) Representative image of IHC analysis of SFRP1, WNT7B, and c-JUN in the retrospectively collected advanced-stage oral SCC patient samples and normal oral mucosa samples (adjacent margin)

f) Dot plot representing the H-score of SFRP1 marker based on the intensity of the staining, advanced-stage skin (n=28) and advanced-stage oral SCC patient samples (n=59), and normal skin (n=10) and oral mucosa (n=12) (adjacent margin), mean ± SEM, two-tailed Mann-Whitney U test

g) Dot plot representing the H-score of WNT7B marker based on the intensity of the staining, advanced-stage skin (n=28) and advanced-stage oral SCC patient samples (n=59), and normal skin (n=10) and oral mucosa (n=12) (adjacent margin), mean ± SEM, two-tailed Mann-Whitney U test

h) Dot plot representing the H-score of c-JUN marker based on the intensity of the staining, advanced-stage skin (n=28) and advanced-stage oral SCC patient samples (n=59), and normal skin (n=10) and oral mucosa (n=12) (adjacent margin), mean ± SEM, two-tailed Mann-Whitney U test

Source data are provided as a Source Data file

ARTICLE IN PRESS

ARTICLE IN PRESS

Figure 2: Loss of SFRP1 increases non-canonical Wnt signaling and glycolytic rate in skin SCC cell line CSCs

a) Representative image of flow cytometry analysis between CSCs (CD133+) and non-CSCs (CD133-) sorted from the A3886 and HEKa cell lines

b) Representative image of spheroids from human skin SCC CSCs and non-CSCs population from A3886 cell line

c) Graphical representation of the number of spheroid forms in CSCs and non-CSCs population after 7 days, n=3 biological replicates, mean ± SEM, two-tailed t-test

d) Serial transplantation assay by subcutaneous injection of the 20,000 FACS-sorted CSCs population in the NOD/SCID mice, n=4

e) Graphical representation of tumor volume in NOD/SCID mice, 20,000 FACS-sorted CSCs serially transplanted three consecutive times, mean ± SEM, two-way ANOVA, n=4 biological replicates

f) Gene expression analysis of the CSCs and non-CSCs by Real-Time PCR, n=3 biological replicates, mean ± SEM, two-tailed multiple t-test followed by Holm-Bonferroni correction, $*P=0.05$, $**P=0.01$, $***P=0.001$

g) Glycolytic rate measurement of A3886 skin SCC cell line by Seahorse analysis, n=3 biological replicates, mean ± SEM, two-tailed t-test

h) Representative image of western blot analysis of non-canonical Wnt signaling between skin SCC cell line (A3886) CSCs and non-CSCs

i) Densitometric analysis of western blot, mean ± SEM, two-tailed multiple t-test followed by Holm-Bonferroni correction, $*P=0.05$, $**P=0.01$, $***P=0.001$, n=3 biological replicates

j) LDH activity assay in skin SCC cell line (A3886) CSCs and non-CSCs, mean ± SEM, two-tailed t-test, n=3 biological replicates

Source data are provided as a Source Data file

ARTICLE IN PRESS

ARTICLE IN PRESS

Figure 3: Sfrp1 knockout increases non-canonical Wnt signaling in murine skin SCC tumor and human skin SCC cell line

a) Representative image of IFA of K14 and VIMENTIN in DMBA/TPA-induced WT SCC, Sfrp1+/- SCC, and Sfrp1-/- SCC tumors

b) Representative image of IFA of K14 and VIMENTIN in WT CSCs, Sfrp1+/- CSCs and Sfrp1-/- CSCs

c) Dot plot showing the number of keratin pearls analyzed, mean ± SEM, a two-tailed t-test was used for the analysis, n=3 biological replicates.

d) Dot plot showing the overlap coefficient of K14 and VIMENTIN in SCC tumors, mean ± SEM, two-tailed Mann-Whitney U test, n=3 biological replicates

e) Overlap coefficient of K14 and VIM plotted as a dot plot, n=3 biological replicates, 50 different cells were quantified in each group, Mean ± SEM, two-tailed Mann-Whitney U test

f) Gene expression analysis of Wnt ligands in WT SCC, Sfrp1+/- SCC, and Sfrp1-/- SCC tumors, n=3 biological replicates, mean ± SEM, two-tailed multiple t-test followed by Holm-Bonferroni correction, **P*=0.05, ***P* =0.01, ****P* =0.001

g) Gene expression analysis of Wnt ligands in the HEKa and A3886 cell lines, n=3 biological replicates, mean ± SEM, two-tailed multiple t-test followed by Holm-Bonferroni correction, **P*=0.05, ***P* =0.01, ****P* =0.001

h) ChIP-qPCR of *c-JUN* on the promoter region of *SOX2* in the skin SCC cell line (A3886), n=3 biological replicates, mean ± SEM, two-tailed t-tests

i) Representative image of a western blot showing the non-canonical Wnt signaling in WT SCC, Sfrp1+/- SCC, and Sfrp1-/- SCC tumors

j) Densitometric analysis of western blot, n=3 biological replicates, mean ± SEM, two-tailed multiple t-test followed by Holm-Bonferroni correction, **P*=0.05, ***P*= 0.01, ****P*= 0.001

k) Representative image of a western blot showing the non-canonical Wnt signaling in HEKa and A3886 cell lines

l) Densitometric analysis of western blot HEKa and A3886 cell lines, n=3 biological replicates, mean ± SEM, two-tailed multiple t-test followed by Holm-Bonferroni correction, **P*=0.05, ***P* =0.01, ****P* =0.001

Source data are provided as a Source Data file

ARTICLE IN PRESS

Figure 4: Sfrp1 overexpression reduces EMT, tumorigenic potential, and non-canonical Wnt signaling in human skin SCC cell line

a) Representative image of IFA of BrdU +ve cells in A3886 VC and A3886 Sfrp1 OE cell lines

b) The dot plot shows the percentage of BrdU +ve cells per field in A3886 VC and A3886 Sfrp1 OE; n=3 biological replicates, mean ± SEM, and two-tailed t-test

c) *In vivo* tumorigenesis assay of one million A3886 VC and A3886 Sfrp1 OE cells by injecting subcutaneously in NOD/SCID mice, n=5

d) Graphical representation of tumor volume of A3886 VC and A3886 Sfrp1 OE cell lines in NOD/SCID mice at various time points, mean ± SEM, two-way ANOVA, n=5 biological replicates

e) Representative image of western blot analysis of non-canonical Wnt signaling between A3886 VC and A3886 Sfrp1 OE cell lines

f) Densitometric analysis of western blot, n=3 biological replicates, mean ± SEM, two-tailed multiple t-test followed by Holm-Bonferroni correction, **P*=0.05, ***P*=0.01, ****P*=0.001

g) Gene expression of EMT markers in A3886 VC and A3886 Sfrp1 OE cell lines by Real Time-PCR, n=3 biological replicates, mean ± SEM, two-tailed multiple t-test followed by Holm-Bonferroni correction, **P*=0.05, ***P*=0.01, ****P*=0.001

h) Representative image of IFA of EMT markers VIMENTIN, E-CADHERIN, TWIST1, KERATIN-8, and stemness marker SOX2 in A3886 VC and A3886 Sfrp1 OE NOD/SCID mice tumors

i) ChIP-qPCR analysis of c-*JUN* on the *VIMENTIN, TWIST1, ZEB1, CCNE1, CDK6* and *SOX2* promoter region in A3886 VC and A3886 Sfrp1 OE cell lines, n=3 biological replicates, mean ± SEM, two-tailed multiple t-test followed by Holm-Bonferroni correction

Source data are provided as a Source Data file

ARTICLE IN PRESS

ARTICLE IN PRESS

Figure 5: Sfrp1 overexpression reduces the hybrid EMT, tumorigenesis, and metastasis in human skin SCC cell line CSCs

a) Representative image of FACS analysis of A3886 VC and A3886 Sfrp1 OE sorted CSCs

b) Graphical representation between A3886 Sfrp1 OE CSCs and A3886 VC CSCs, n=3 biological replicates, mean ± SEM, two-tailed t-test

c) *In vivo* tumorigenesis assay of FACS sorted 20,000 A3886 VC and A3886 Sfrp1 OE CSCs in the NOD SCID mice, n=6

d) Graphical representation of tumor volume at different time points, mean ± SEM, two-way ANOVA, n=6 biological replicates

e) Representative image of IFA of K14 and VIMENTIN in the A3886 VC and A3886 Sfrp1 OE CSCs

f) Dot plot represented the overlap coefficient between K14 and VIMENTIN between A3886 VC and A3886 Sfrp1 OE CSCs, n=3 biological replicates, mean ± SEM, two-tailed t-test

g) Representative image of PET activity of the A3886 VC and A3886 Sfrp1 OE CSCs injected in the NOD/SCID mouse

h) Graphical representation of PET activity in the A3886 VC and A3886 Sfrp1 OE NOD/SCID mice, n=3 biological replicates, mean ± SEM, two-tailed t-test

i) Representative image of lung metastasis by intravenous injection of 20,000 A3886 VC and A3886 Sfrp1 OE CSCs metastasized in the lungs of NOD/SCID mice

j) Representative image of H&E staining of the lung metastasized colonies in the A3886 VC and A3886 Sfrp1 OE NOD/SCID mice

k) Number of lung metastasized colonies arising from the 20,000 A3886 VC and A3886 Sfrp1 OE CSCs, mean ± SEM, two-tailed t-test, n=6 biological replicates

l) Graphical representation of %lung metastases in the A3886 VC and A3886 Sfrp1 OE NOD/SCID mice, n=6 biological replicates, mean ± SEM, two-tailed t-test

Source data are provided as a Source Data file

ARTICLE IN PRESS

Figure 6: Sfrp1 overexpression reduces in vivo tumorigenesis and metastatic potential in oral SCC cell lines

a) Representative image of western blot analysis of non-canonical Wnt signaling in ACOSC4 VC, ACOSC4 Sfrp1 OE, ACOSC3 VC, ACOSC3 Sfrp1 OE, ACOSC16 VC, and ACOSC16 Sfrp1 OE cell lines

b) Densitometric analysis of non-canonical Wnt signaling in ACOSC4 VC, ACOSC4 Sfrp1 OE, ACOSC3 VC, ACOSC3 Sfrp1 OE, ACOSC16 VC, and ACOSC16 Sfrp1 OE, NOD/SCID mice, mean ± SEM, two-tailed multiple t-test followed by Holm-Bonferroni correction, **P* =0.05, ***P*= 0.01, ****P*= 0.001, n=3 biological replicates

c) *In vivo* tumorigenesis assay of one million ACOSC4 VC, ACOSC4 Sfrp1 OE, ACOSC3 VC, ACOSC3 Sfrp1 OE, ACOSC16 VC and ACOSC16 Sfrp1 OE cell lines, n=3

d) Graphical representation of tumor volumes of ACOSC4 VC, ACOSC4 Sfrp1 OE, ACOSC3 VC, ACOSC3 Sfrp1 OE, ACOSC16 VC, and ACOSC16 Sfrp1 OE, NOD/SCID mice, mean ± SEM, two-way ANOVA, **P* =0.05, ***P*= 0.01, ****P*= 0.001, n=3 biological replicates

e) ChIP-qPCR analysis of c-*JUN* on the promoter region of *SOX2* in the ACOSC4 VC, ACOSC4 Sfrp1 OE, ACOSC3 VC, ACOSC16 Sfrp1 OE, ACOSC3 VC, and ACOSC16 Sfrp1 OE cell lines, n=3 biological replicates, mean ± SEM, two-tailed multiple t-test followed by Holm-Bonferroni correction

f) Representative image of PET activity of ACOSC4 VC, ACOSC4 Sfrp1 OE, ACOSC3 VC, ACOSC3 Sfrp1 OE, ACOSC16 VC, and ACOSC16 Sfrp1 OE NOD/SCID mice

Source data are provided as a Source Data file

Figure 7: EZH2-mediated loss of SFRP1 in the skin and oral SCC cell lines

a) GSEA showing the enrichment of PRC2-mediated DNA and histone methylation in the human skin SCC FACS-sorted CSCs and non-CSCs

b) Validation of epigenetic modifiers in CSCs (CD133+) isolated from the advanced-stage skin SCC patient biopsy and normal skin tissue (adjacent margin) by Real-Time PCR, n=3 biological replicates, mean ± SEM, two-tailed multiple t-test followed by Holm-Bonferroni correction

c) Representative image of IHC of EZH2 in the retrospectively collected advanced-stage skin SCC patient samples and normal skin samples (adjacent margin)

ARTICLE IN PRESS

d) Dot plot representing the H-score of EZH2 marker based on the intensity of the staining, advanced-stage skin (n=28) and normal skin (adjacent margin) (n=10), mean ± SEM, two-tailed Mann-Whitney U test

e) Representative image of IHC of EZH2 in the retrospectively collected advanced-stage oral SCC patient samples and normal oral mucosa samples (adjacent margin)

f) Dot plot representing the H-score of EZH2 marker based on the intensity of the staining, advanced-stage oral SCC patient samples (n=59), and oral mucosa (n=12), mean ± SEM, Mann-Whitney U test

g) ChIP-qPCR analysis of H3K27me3 mark on the *SFRP1* promoter region of human skin SCC A3886 cell line, n=3 biological replicates, mean ± SEM, two-tailed t-test

h) Representative image of western blot of EZH2, H3K27me3, and H3K27ac in CSCs and non-CSCs

i) Densitometric analysis of western blot, n=3 biological replicates, mean ± SEM, two-tailed multiple t-test followed by Holm-Bonferroni correction

j) ChIP-qPCR analysis of H3K27me3 mark on the *SFRP1* promoter region of OSCC cell lines, n=3 biological replicates, mean ± SEM, two-tailed t-test.

k) Representative image of western blot analysis of EZH2, H3K27me3, and H3K27ac in OSCC cell lines

l) Densitometric analysis of western blot, n=3 biological replicates, mean ± SEM, two-tailed multiple t-test followed by Holm-Bonferroni correction, **P*=0.05, ***P* =0.01, ****P* =0.001

Source data are provided as a Source Data file

Figure 8: DAC reduces histone methylation and glycolysis due to the increased SFRP1 levels in the skin and oral SCC cell lines

a) ChIP-qPCR of the H3K27me3 on the *SFRP1* promoter region after DAC treatment in A3886 cell line, n=3 biological replicates, mean ± SEM, two-tailed t-test

b) ChIP-qPCR of H3K27me3 on the *SFRP1* promoter region after DAC treatment in OSCC cell lines, n=3 biological replicates, mean ± SEM, two-tailed t-test

c) Representative image of western blot analysis of H3K27me3 and H3K27ac in DAC treatment in A3886 skin cell line

ARTICLE IN PRESS

d) Densitometric analysis of western blot, n=3 biological replicates, mean ± SEM, two-tailed multiple t-test followed by Holm-Bonferroni correction

e) Representative image of western blot analysis of H3K27me3 and H3K27ac after DAC treatment in OSCC cell lines

f) Densitometric analysis of western blot, n=3 biological replicates, mean ± SEM, two-tailed multiple t-test followed by Holm-Bonferroni correction

g) GSEA showing the enrichment of hypoxia in the human skin SCC cell line (A3886) CSCs and non-CSCs

h) ChIP-qPCR of the *SOX2* on the *HIF1*α promoter region after DAC treatment to the A3886 cell line, n=3 biological replicates, mean ± SEM, two-tailed t-test

i) ChIP-qPCR of the *SOX2* on the *HIF1*α promoter region after DAC treatment of the OSCC cell lines, n=3 biological replicates, mean ± SEM, two-tailed multiple t-test followed by Holm-Bonferroni correction

j) GSEA showed enrichment of glycolysis in the human skin SCC (A3886) CSCs and non-CSCs

k) String analysis of *HIF1*α and glycolytic genes (*HK2*, *LDHA*, *SLC2A2)* and stemness marker (*SOX2*)

l) ChIP-qPCR of *HIF1*α and *HK2*, *LDHA* and *SLC2A2* in DAC treatment in skin SCC cell line (A3886), n=3 biological replicates, mean ± SEM, two-tailed multiple t-test followed by Holm-Bonferroni correction

m) ChIP-qPCR analysis of *HIF1*α and *HK2*, *LDHA* and *SLC2A2* in DAC treatment OSCC cell lines, n=3 biological replicates, mean ± SEM, two-tailed multiple t-test followed by Holm-Bonferroni correction

Source data are provided as a Source Data file

Figure 9: DAC treatment reduces hypoxia and glycolysis in skin and oral SCC cell lines

a) Representative image of western blot analysis of HK2 and LDHA levels in the DAC-treated A3886 skin SCC cell line

b) Densitometric analysis of western blot, n=3 biological replicates, mean ± SEM, two-tailed multiple t-test followed by Holm-Bonferroni correction

c) Representative image of western blot analysis of HK2 and LDHA levels in the DAC treatment of OSCC cell lines

ARTICLE IN PRESS

d) Densitometric analysis of western blot, n=3 biological replicates, mean ± SEM, two-tailed multiple t-test followed by Holm-Bonferroni correction

e) Lactate dehydrogenase activity in the A3886 VC and A3886+DAC, n=3 biological replicates, mean ± SEM, two-way ANOVA

f) Lactate levels in the A3886 VC and A3886+DAC, n=3 biological replicates, mean ± SEM, two-way ANOVA

g) Pyruvate levels in the A3886 VC and A3886+DAC, n=3 biological replicates, mean ± SEM, two-way ANOVA

h) Acetyl Co-A levels in the A3886 VC and A3886+DAC, n=3 biological replicates, mean ± SEM, two-way ANOVA

i) Lactate dehydrogenase activity in the OSCC cell lines and DAC-treated OSCC cell lines, n=3 biological replicates, mean ± SEM, two-way ANOVA

j) Lactate levels in the OSCC cell lines and DAC-treated OSCC cell lines, n=3 biological replicates, mean ± SEM, two-tailed t-test, two-way ANOVA

k) Pyruvate levels in the OSCC cell lines and DAC-treated OSCC cell lines, n=3 biological replicates, mean ± SEM, two-way ANOVA

l) Acetyl Co-A levels in the OSCC cell lines and DAC-treated OSCC cell lines, n=3 biological replicates, mean ± SEM, two-way ANOVA

Source data are provided as a Source Data file

ARTICLE IN PRESS

Figure 10: DAC and RAC1i treatment reduces *in vivo* tumorigenic potential in skin and oral SCCs

a) *In vivo* tumorigenesis assay by injecting the A3886 skin SCC cell line and administration of the DAC intraperitoneal in the NOD/SCID mice, n=5

b) Representation of the tumor volume of A3886 and A3886 + DAC tumors, mean ± SEM, two-way ANOVA, n=5 biological replicates

c) *In vivo* tumorigenesis assay of OSCC cell lines and administration of the DAC intraperitoneal in the NOD/SCID mice, n=5

d) Representation of the tumor volume of OSCC cell lines and after administration of the DAC in the NOD/SCID mice, n=5 biological replicates, mean ± SEM, two-way ANOVA

ARTICLE IN PRESS

e) *In vivo* tumorigenesis assay by injecting the A3886 skin SCC cell line and administration of the DAC, RAC1i, and DAC & RAC1i intraperitoneal in the NOD/SCID mice, n=5

f) Representation of the tumor volume of A3886 skin SCC cell line after treatment with DAC, RAC1i, and DAC & RAC1i in the NOD/SCID mice, mean ± SEM, two-way ANOVA, n=5 biological replicates

g) *In vivo* tumorigenesis assay by injecting the ACOSC4 OSCC cell line and administration of the DAC, RAC1i, and DAC & RAC1i intraperitoneal in the NOD/SCID mice, n=5

h) Representation of the ACOSC4 tumor volume after treatment with DAC, RAC1i, and DAC & RAC1i mean ± SEM, two-way ANOVA, n=5 biological replicates

i) *In vivo* tumorigenesis assay by injecting the ACOSC3 OSCC cell line and administration of the DAC, RAC1i, and DAC & RAC1i intraperitoneal in the NOD/SCID mice, n=5 mice/group

j) Representation of the ACOSC3 tumor volume after treatment with DAC, RAC1i, and DAC & RAC1i mean ± SEM, two-way ANOVA, n=5 biological replicates

k) Graphical model representing the histone and DNA methylation leads to loss of SFRP1, which in turn activates the non-canonical Wnt signaling that promotes cancer stemness, glycolysis, in vivo tumorigenesis, and metastatic potential. However, DAC treatment reduces histone and DNA methylation, restoring SFRP1 levels, which in turn reduces non-canonical Wnt signaling, stemness, glycolysis, in vivo tumorigenesis, and metastatic potential (Created with https://biorender.com/j34ubni)

Source data are provided as a Source Data file

ARTICLE IN PRESS

Editor Summary:

Squamous cell carcinomas (SCCs) show poor survival due to the presence of cancer stem cells (CSCs). Here, the authors delineate the molecular mechanism underlying SCC progression by identifying a crosstalk of epigenetic-signaling metabolism axis, which showed global hypermethylation activates non-canonical Wnt signaling, in turn activating glycolysis in skin and oral SCC.

Peer Review Information:

Nature Communications thanks Bin Zhang, Manish Bais and the other anonymous reviewers for their contribution to the peer review of this work. [A peer review file is available.]

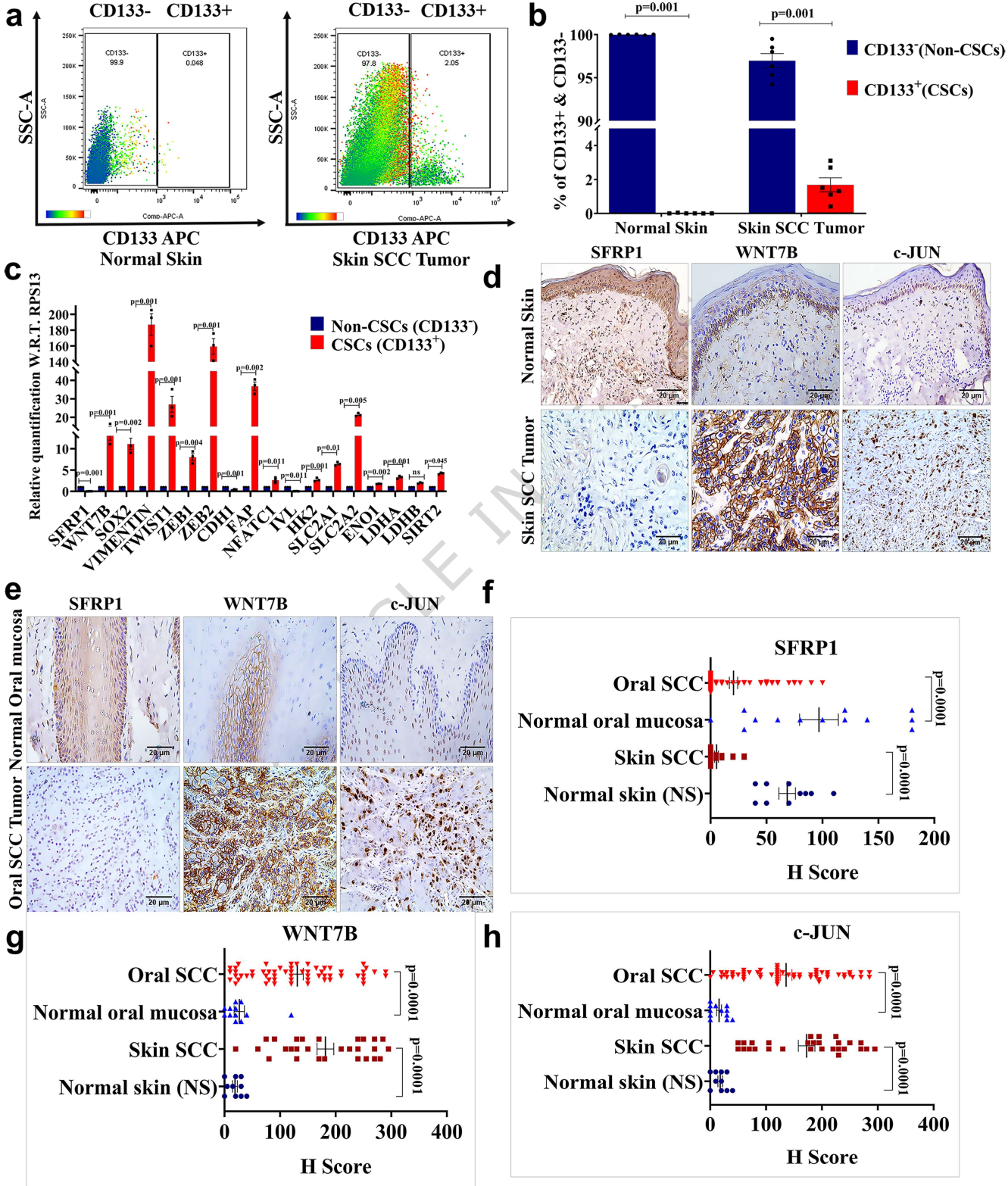
a
CD133- CD133+
SSC-A
CD133- 99.9
CD133+ 0.048
CD133 APC
Normal Skin
CD133- CD133+
CD133- 97.8
CD133+ 2.05
CD133 APC
Skin SCC Tumor
b
p=0.001
p=0.001
% of CD133+ & CD133-
CD133-(Non-CSCs)
CD133+(CSCs)
Normal Skin
Skin SCC Tumor
c
Relative quantification W.R.T. RPS13
Non-CSCs (CD133-)
CSCs (CD133+)
SFRP1
WNT7B
SOX2
VIMENTIN
TWIST1
ZEB1
ZEB2
CDH1
FAP
NFATC1
IVL
HK2
SLC2A1
SLC2A2
ENO1
LDHA
LDHB
SIRT2
d
SFRP1
WNT7B
c-JUN
Normal Skin
Skin SCC Tumor
e
SFRP1
WNT7B
c-JUN
Normal Oral mucosa
Oral SCC Tumor
f
SFRP1
Oral SCC
Normal oral mucosa
Skin SCC
Normal skin (NS)
p=0.0001
p=0.0001
H Score
g
WNT7B
Oral SCC
Normal oral mucosa
Skin SCC
Normal skin (NS)
p=0.0001
p=0.0001
H Score
h
c-JUN
Oral SCC
Normal oral mucosa
Skin SCC
Normal skin (NS)
p=0.0001
p=0.0001
H Score

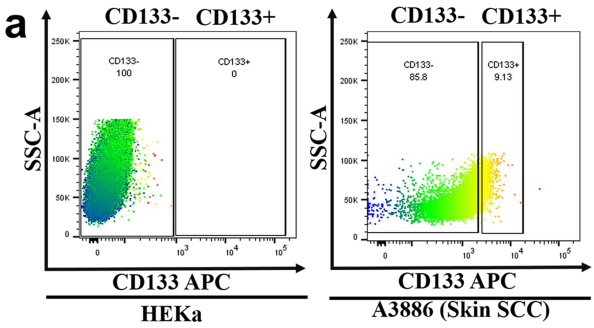
a
CD133- CD133+
CD133- 100
CD133+ 0
SSC-A
CD133 APC
HEKa
CD133- CD133+
CD133- 85.8
CD133+ 9.13
SSC-A
CD133 APC
A3886 (Skin SCC)

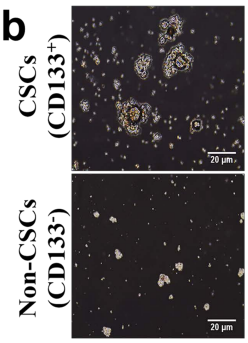
b
CSCs (CD133+)
Non-CSCs (CD133-)
20 µm
20 µm

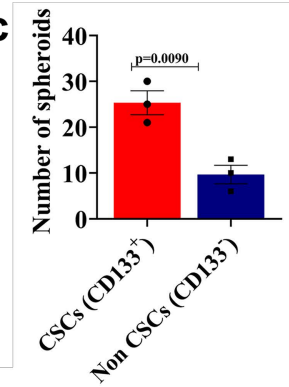
c
Number of spheroids
p=0.0090
CSCs (CD133+)
Non CSCs (CD133-)

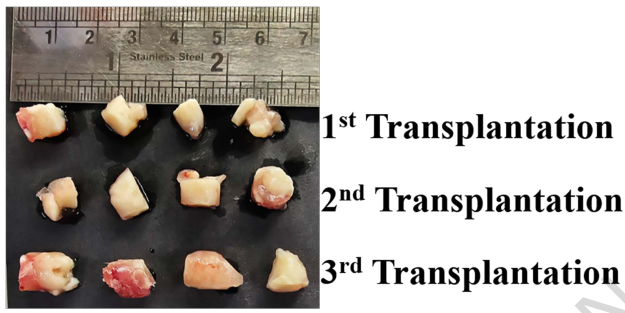
d
Stainless Steel
1st Transplantation
2nd Transplantation
3rd Transplantation

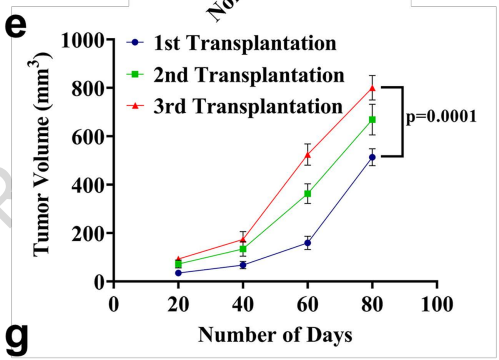
e
1st Transplantation
2nd Transplantation
3rd Transplantation
p=0.0001
Tumor Volume (mm3)
Number of Days

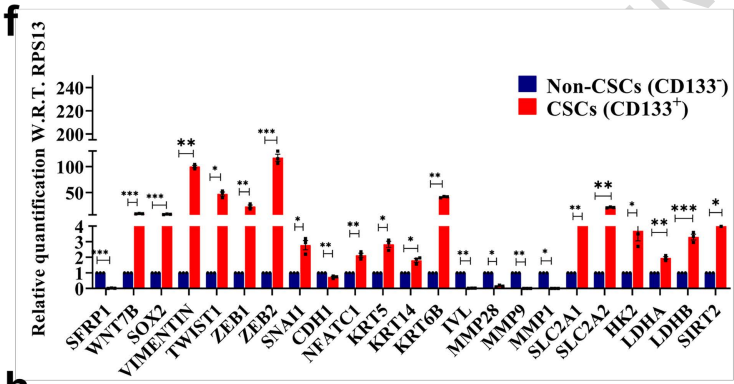
f
Non-CSCs (CD133-)
CSCs (CD133+)
Relative quantification W.R.T. RPS13
SFRP1
WNT7B
SOX2
VIMENTIN
TWIST1
ZEB1
ZEB2
SNAI1
CDH1
NFATC1
KRT5
KRT14
KRT6B
IVL
MMP28
MMP9
MMP1
SLC2A1
SLC2A2
HK2
LDHA
LDHB
SIRT2

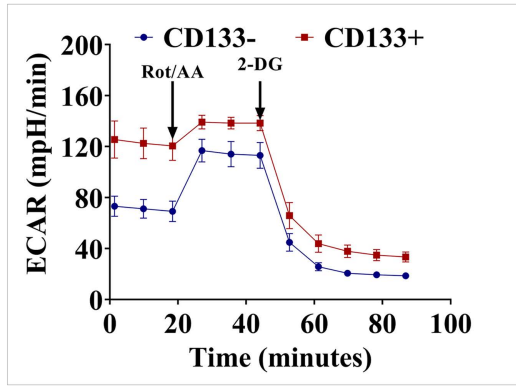
g
CD133-
CD133+
Rot/AA
2-DG
ECAR (mpH/min)
Time (minutes)

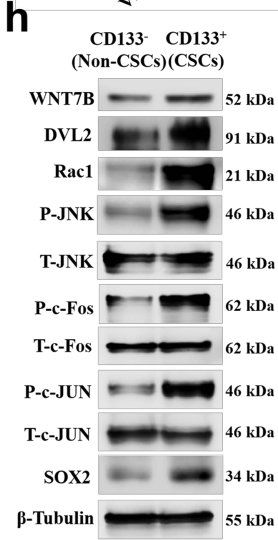
h
CD133- (Non-CSCs)
CD133+ (CSCs)
WNT7B 52 kDa
DVL2 91 kDa
Rac1 21 kDa
P-JNK 46 kDa
T-JNK 46 kDa
P-c-Fos 62 kDa
T-c-Fos 62 kDa
P-c-JUN 46 kDa
T-c-JUN 46 kDa
SOX2 34 kDa
β-Tubulin 55 kDa

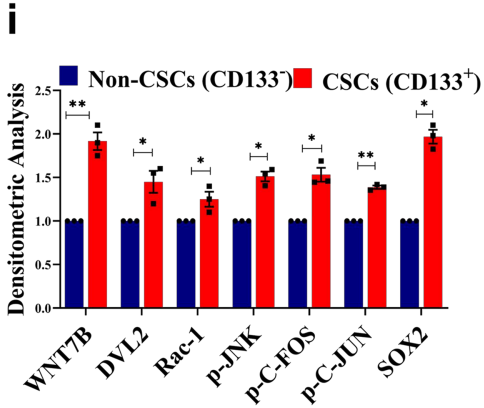
i
Non-CSCs (CD133-)
CSCs (CD133+)
Densitometric Analysis
WNT7B
DVL2
Rac-1
p-JNK
p-C-FOS
p-C-JUN
SOX2

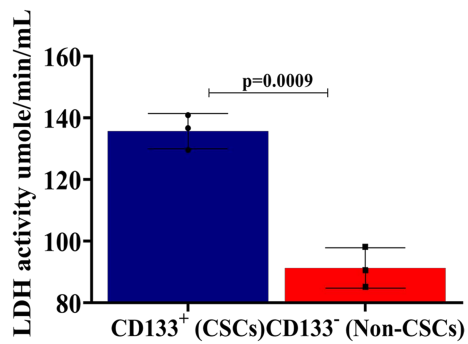
j
p=0.0009
LDH activity umole/min/mL
CD133+ (CSCs)
CD133- (Non-CSCs)

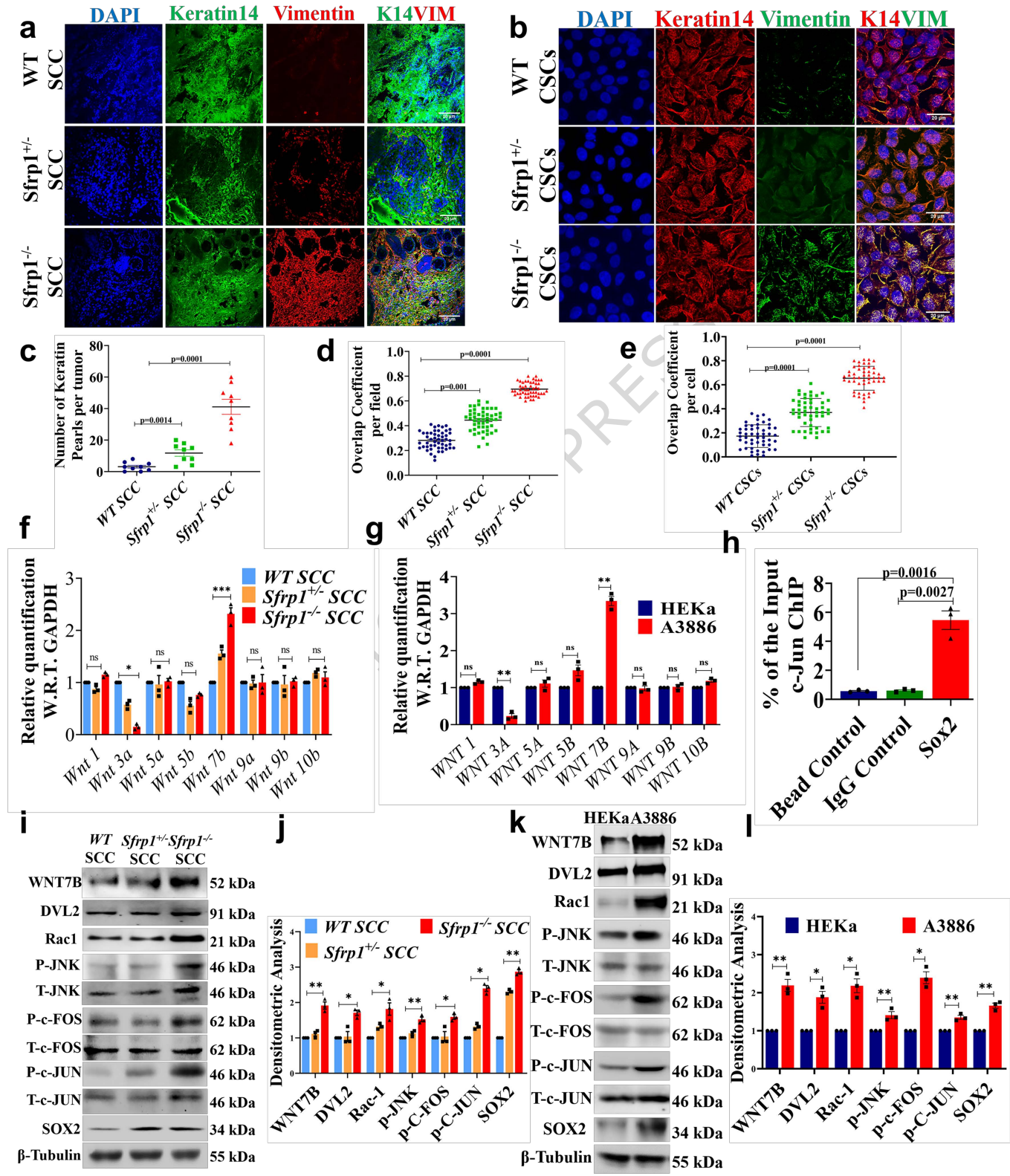
a
DAPI
Keratin14
Vimentin
K14VIM
WT SCC
Sfrp1+/- SCC
Sfrp1-/- SCC
b
DAPI
Keratin14
Vimentin
K14VIM
WT CSCs
Sfrp1+/- CSCs
Sfrp1-/- CSCs
c
Number of Keratin Pearls per tumor
p=0.0001
p=0.0014
WT SCC
Sfrp1+/- SCC
Sfrp1-/- SCC
d
Overlap Coefficient per field
p=0.0001
p=0.001
WT SCC
Sfrp1+/- SCC
Sfrp1-/- SCC
e
Overlap Coefficient per cell
p=0.0001
p=0.0001
WT CSCs
Sfrp1+/- CSCs
Sfrp1+/- CSCs
f
Relative quantification W.R.T. GAPDH
WT SCC
Sfrp1+/- SCC
Sfrp1-/- SCC
Wnt 1
Wnt 3a
Wnt 5a
Wnt 5b
Wnt 7b
Wnt 9a
Wnt 9b
Wnt 10b
g
Relative quantification W.R.T. GAPDH
HEKa
A3886
WNT 1
WNT 3A
WNT 5A
WNT 5B
WNT 7B
WNT 9A
WNT 9B
WNT 10B
h
% of the Input c-Jun ChIP
p=0.0016
p=0.0027
Bead Control
IgG Control
Sox2
i
WT SCC
Sfrp1+/- SCC
Sfrp1-/- SCC
WNT7B 52 kDa
DVL2 91 kDa
Rac1 21 kDa
P-JNK 46 kDa
T-JNK 46 kDa
P-c-FOS 62 kDa
T-c-FOS 62 kDa
P-c-JUN 46 kDa
T-c-JUN 46 kDa
SOX2 34 kDa
β-Tubulin 55 kDa
j
Densitometric Analysis
WT SCC
Sfrp1+/- SCC
Sfrp1-/- SCC
WNT7B
DVL2
Rac-1
p-JNK
p-C-FOS
p-C-JUN
SOX2
k
HEKa
A3886
WNT7B 52 kDa
DVL2 91 kDa
Rac1 21 kDa
P-JNK 46 kDa
T-JNK 46 kDa
P-c-FOS 62 kDa
T-c-FOS 62 kDa
P-c-JUN 46 kDa
T-c-JUN 46 kDa
SOX2 34 kDa
β-Tubulin 55 kDa
l
Densitometric Analysis
HEKa
A3886
WNT7B
DVL2
Rac-1
p-JNK
p-c-FOS
p-C-JUN
SOX2

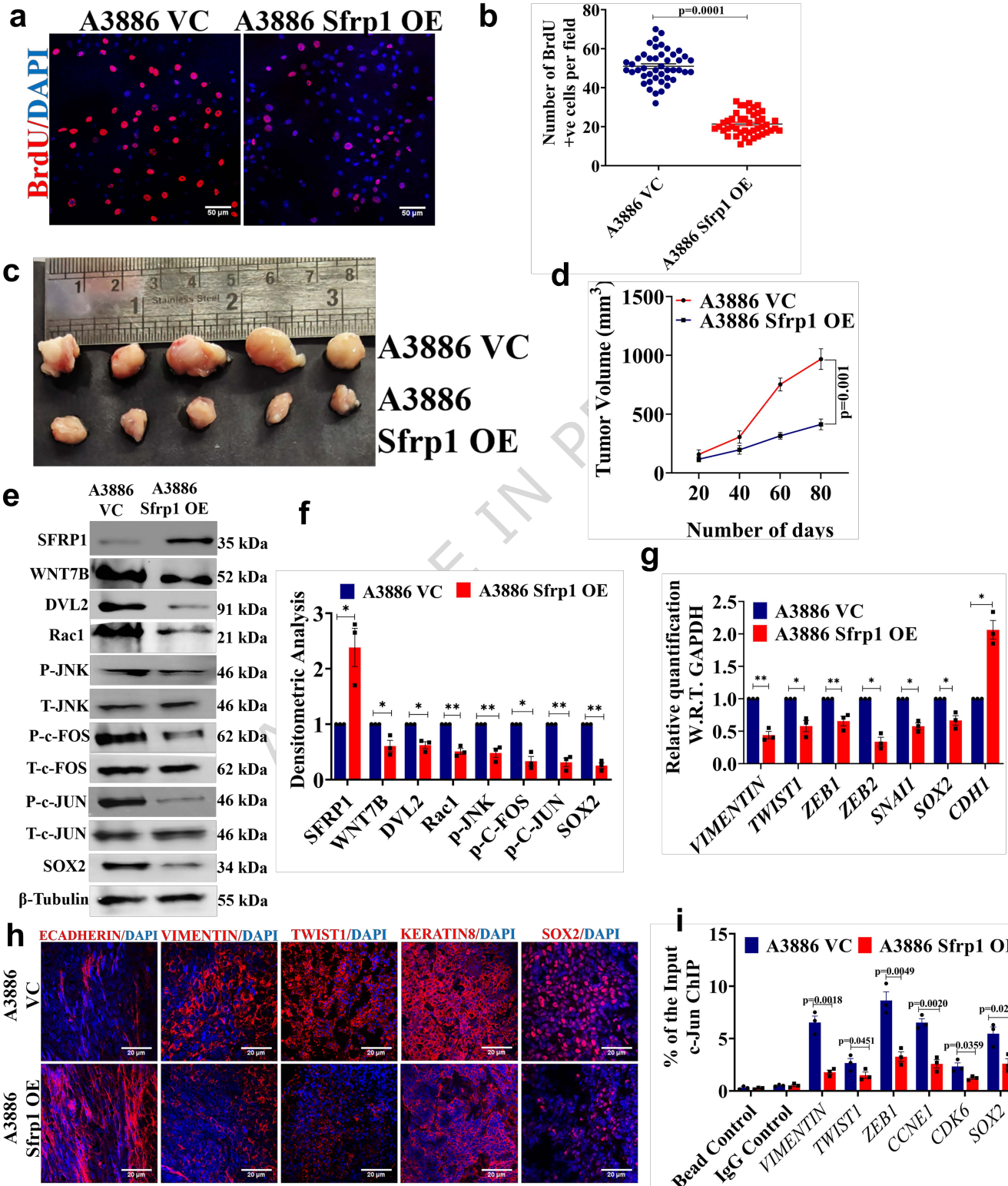
a
A3886 VC
A3886 Sfrp1 OE
BrdU/DAPI
50 μm
b
Number of BrdU +ve cells per field
p=0.0001
A3886 VC
A3886 Sfrp1 OE
c
A3886 VC
A3886 Sfrp1 OE
d
Tumor Volume (mm3)
A3886 VC
A3886 Sfrp1 OE
p=0.001
Number of days
e
A3886 VC
A3886 Sfrp1 OE
SFRP1 35 kDa
WNT7B 52 kDa
DVL2 91 kDa
Rac1 21 kDa
P-JNK 46 kDa
T-JNK 46 kDa
P-c-FOS 62 kDa
T-c-FOS 62 kDa
P-c-JUN 46 kDa
T-c-JUN 46 kDa
SOX2 34 kDa
β-Tubulin 55 kDa
f
Densitometric Analysis
A3886 VC
A3886 Sfrp1 OE
SFRP1
WNT7B
DVL2
Rac1
p-JNK
p-C-FOS
p-C-JUN
SOX2
g
Relative quantification W.R.T. GAPDH
A3886 VC
A3886 Sfrp1 OE
VIMENTIN
TWIST1
ZEB1
ZEB2
SNAI1
SOX2
CDH1
h
ECADHERIN/DAPI
VIMENTIN/DAPI
TWIST1/DAPI
KERATIN8/DAPI
SOX2/DAPI
A3886 VC
A3886 Sfrp1 OE
20 μm
i
% of the Input c-Jun ChIP
A3886 VC
A3886 Sfrp1 OE
p=0.0018
p=0.0451
p=0.0049
p=0.0020
p=0.0359
p=0.0230
Bead Control
IgG Control
VIMENTIN
TWIST1
ZEB1
CCNE1
CDK6
SOX2

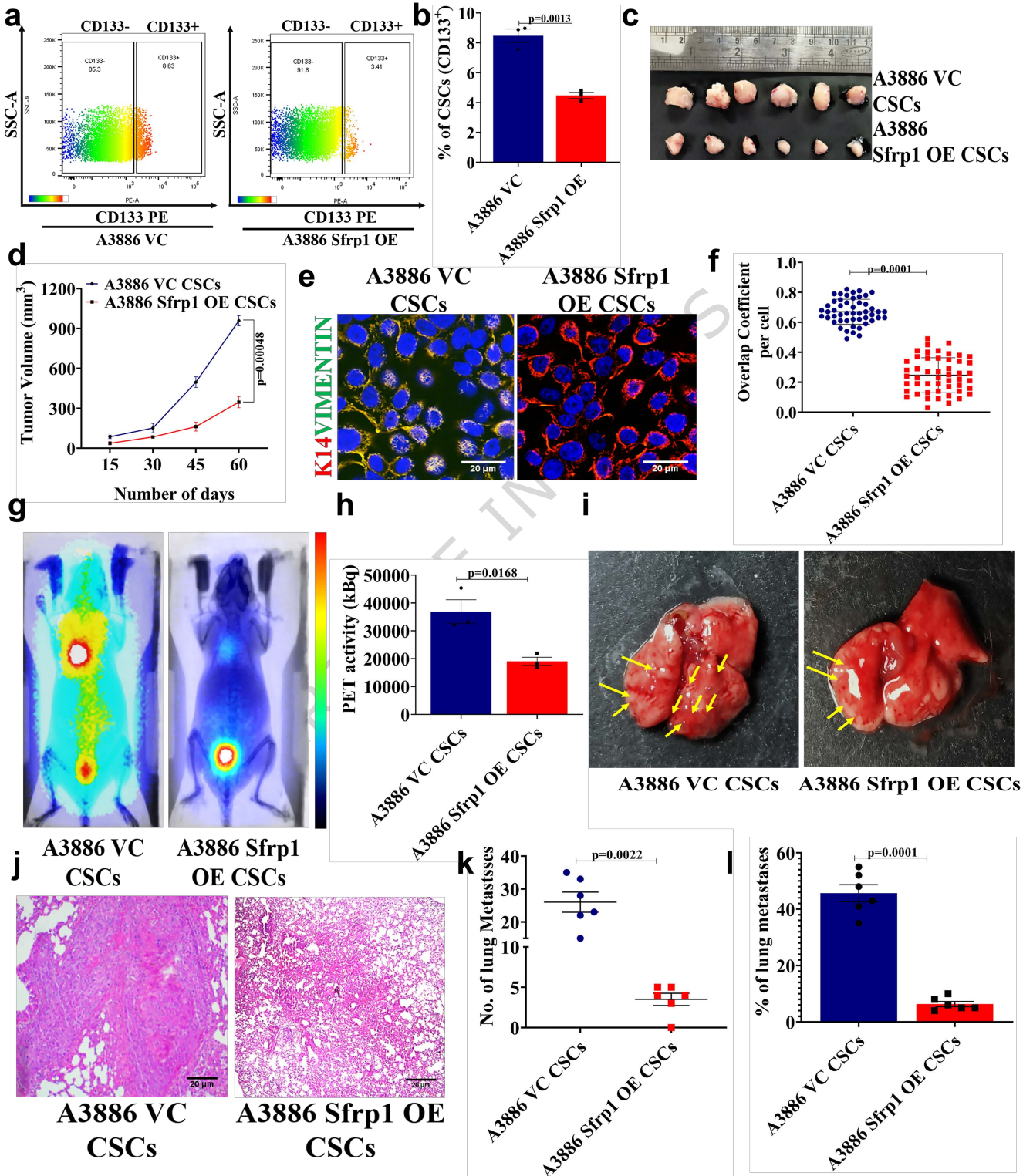
a
CD133-
CD133+
SSC-A
CD133- 85.3
CD133+ 8.63
CD133 PE
A3886 VC
CD133- 91.8
CD133+ 3.41
A3886 Sfrp1 OE
b
% of CSCs (CD133+)
p=0.0013
A3886 VC
A3886 Sfrp1 OE
c
A3886 VC CSCs
A3886 Sfrp1 OE CSCs
d
Tumor Volume (mm3)
A3886 VC CSCs
A3886 Sfrp1 OE CSCs
p=0.00048
Number of days
e
A3886 VC CSCs
A3886 Sfrp1 OE CSCs
K14VIMENTIN
20 µm
f
Overlap Coefficient per cell
p=0.0001
A3886 VC CSCs
A3886 Sfrp1 OE CSCs
g
A3886 VC CSCs
A3886 Sfrp1 OE CSCs
h
PET activity (kBq)
p=0.0168
A3886 VC CSCs
A3886 Sfrp1 OE CSCs
i
A3886 VC CSCs
A3886 Sfrp1 OE CSCs
j
A3886 VC CSCs
A3886 Sfrp1 OE CSCs
20 µm
k
No. of lung Metastsses
p=0.0022
A3886 VC CSCs
A3886 Sfrp1 OE CSCs
l
% of lung metastases
p=0.0001
A3886 VC CSCs
A3886 Sfrp1 OE CSCs

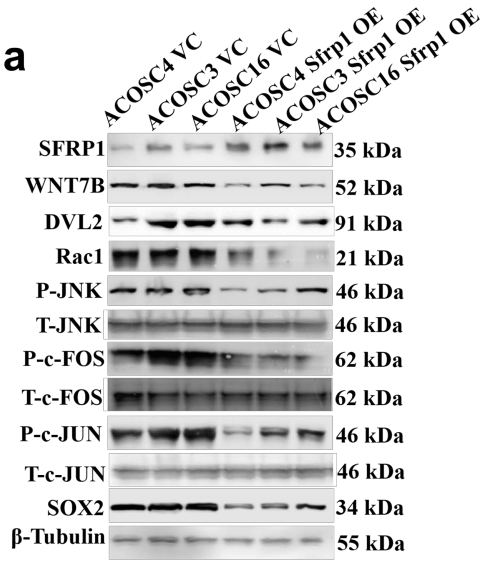
a
ACOSC4 VC
ACOSC3 VC
ACOSC16 VC
ACOSC4 Sfrp1 OE
ACOSC3 Sfrp1 OE
ACOSC16 Sfrp1 OE
SFRP1
WNT7B
DVL2
Rac1
P-JNK
T-JNK
P-c-FOS
T-c-FOS
P-c-JUN
T-c-JUN
SOX2
β-Tubulin
35 kDa
52 kDa
91 kDa
21 kDa
46 kDa
46 kDa
62 kDa
62 kDa
46 kDa
46 kDa
34 kDa
55 kDa

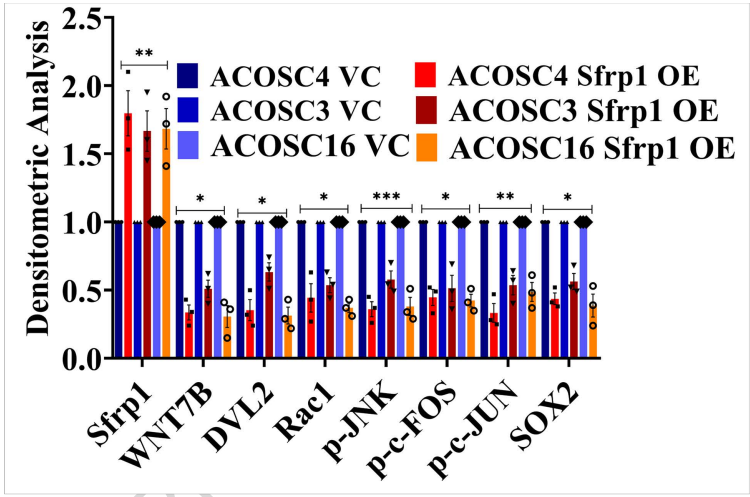
b
Densitometric Analysis
ACOSC4 VC
ACOSC3 VC
ACOSC16 VC
ACOSC4 Sfrp1 OE
ACOSC3 Sfrp1 OE
ACOSC16 Sfrp1 OE
Sfrp1
WNT7B
DVL2
Rac1
p-JNK
p-c-FOS
p-c-JUN
SOX2

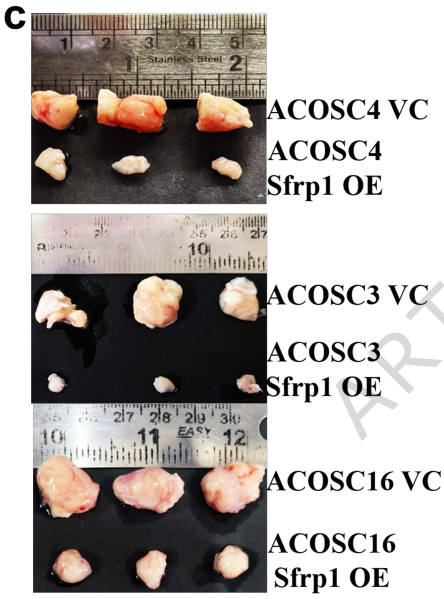
c
ACOSC4 VC
ACOSC4 Sfrp1 OE
ACOSC3 VC
ACOSC3 Sfrp1 OE
ACOSC16 VC
ACOSC16 Sfrp1 OE

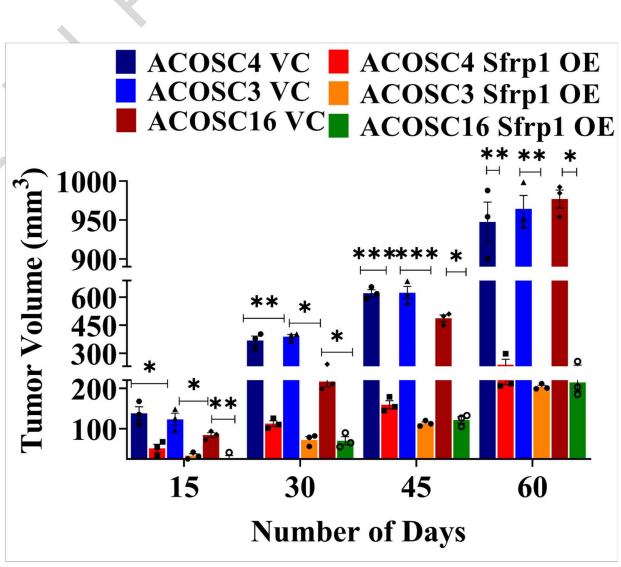
d
ACOSC4 VC
ACOSC3 VC
ACOSC16 VC
ACOSC4 Sfrp1 OE
ACOSC3 Sfrp1 OE
ACOSC16 Sfrp1 OE
Tumor Volume (mm3)
Number of Days

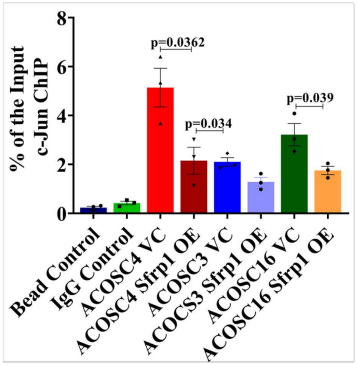
e
% of the Input c-Jun ChIP
p=0.0362
p=0.034
p=0.039
Bead Control
IgG Control
ACOSC4 VC
ACOSC4 Sfrp1 OE
ACOSC3 VC
ACOSC3 Sfrp1 OE
ACOSC16 VC
ACOSC16 Sfrp1 OE

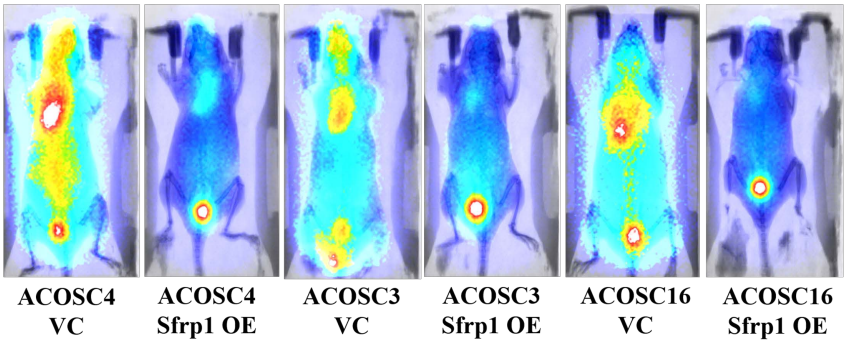
f
ACOSC4 VC
ACOSC4 Sfrp1 OE
ACOSC3 VC
ACOSC3 Sfrp1 OE
ACOSC16 VC
ACOSC16 Sfrp1 OE

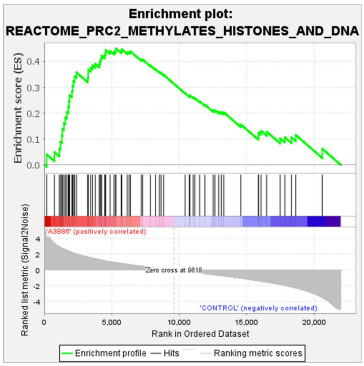

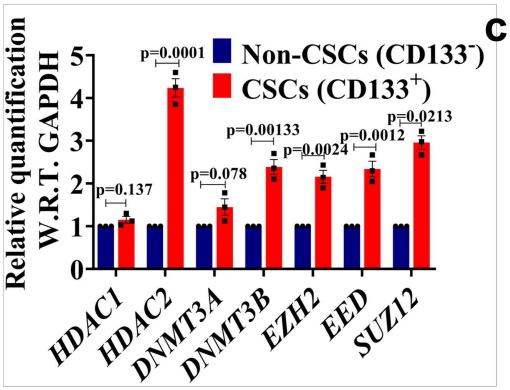

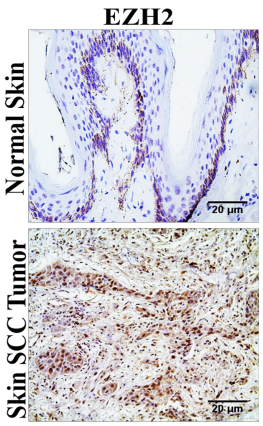

Enrichment of PRC2 Methylation (Histone and DNA)

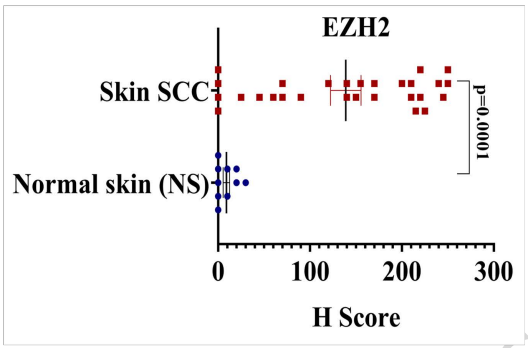

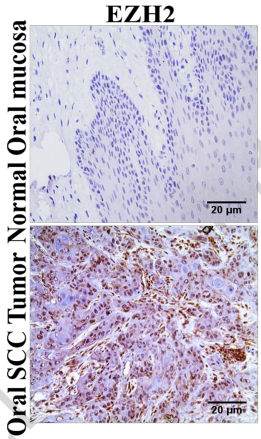

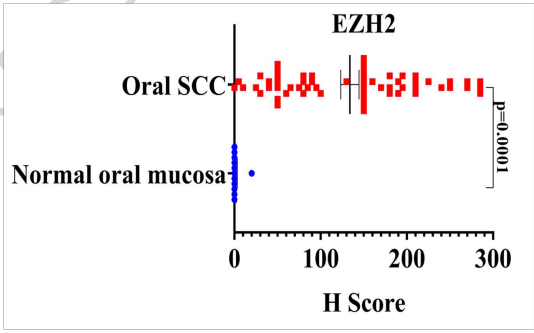

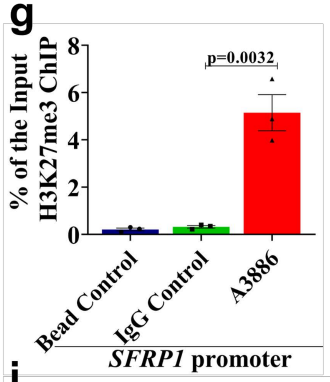

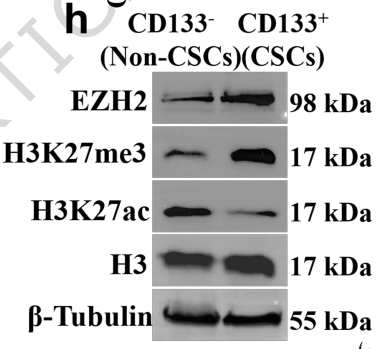

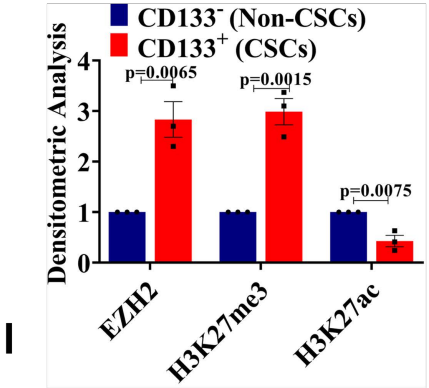

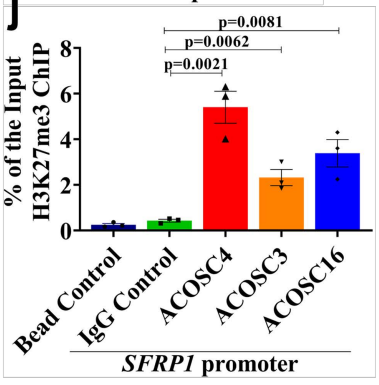

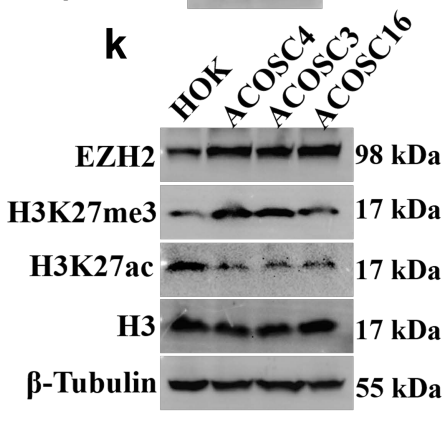

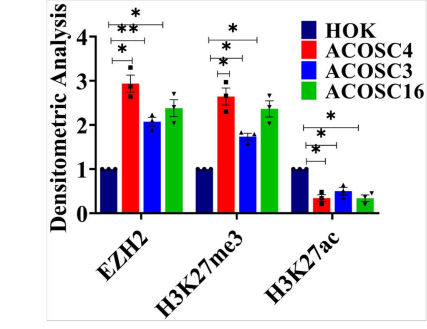

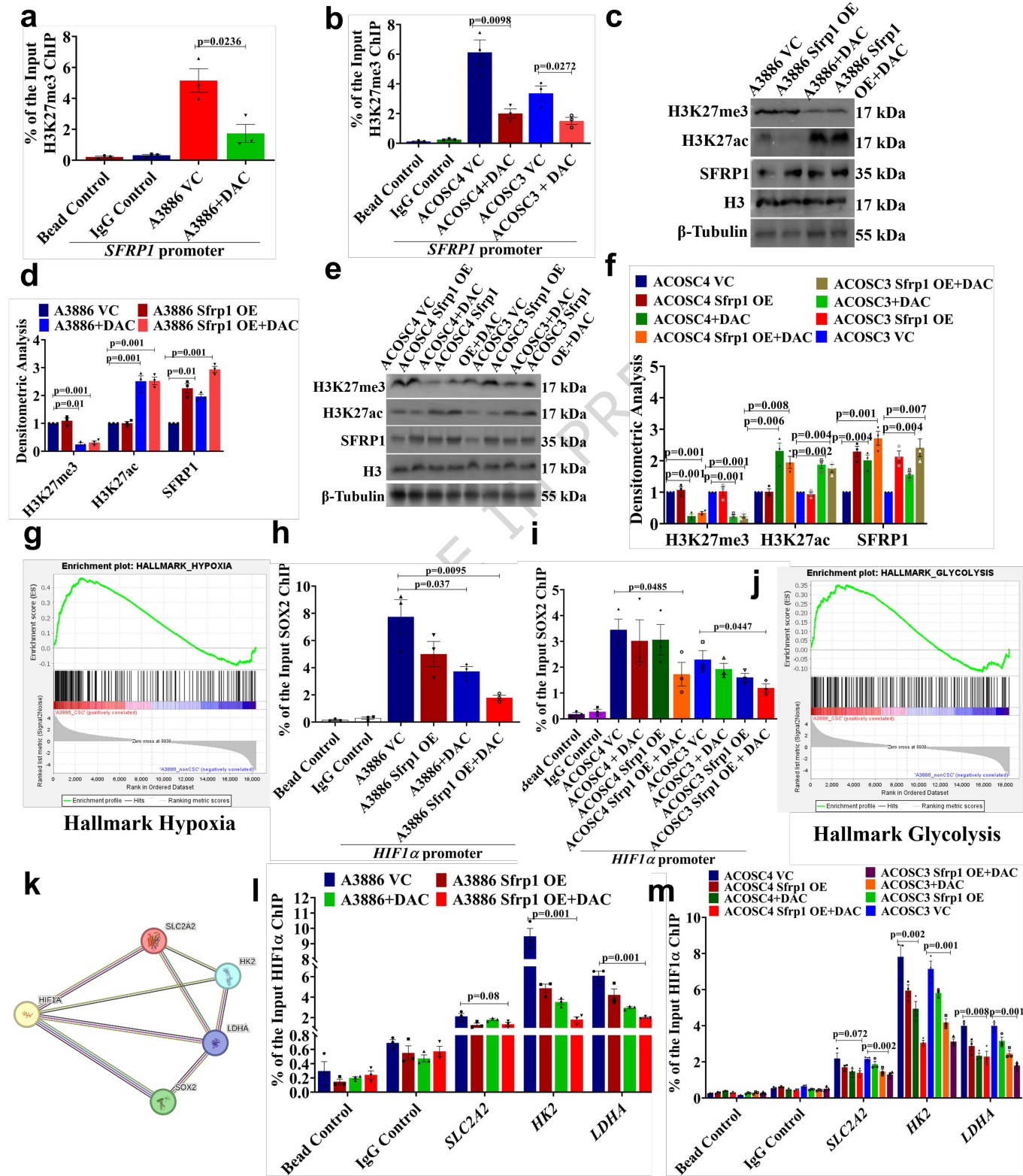
a
% of the Input H3K27me3 ChIP
p=0.0236
Bead Control
IgG Control
A3886 VC
A3886+DAC
SFRP1 promoter
b
% of the Input H3K27me3 ChIP
p=0.0098
p=0.0272
Bead Control
IgG Control
ACOSC4 VC
ACOSC4+DAC
ACOSC3 VC
ACOSC3 + DAC
SFRP1 promoter
c
A3886 VC
A3886 Sfrp1 OE
A3886+DAC
A3886 Sfrp1 OE+DAC
H3K27me3
H3K27ac
SFRP1
H3
β-Tubulin
17 kDa
17 kDa
35 kDa
17 kDa
55 kDa
d
A3886 VC
A3886 Sfrp1 OE
A3886+DAC
A3886 Sfrp1 OE+DAC
Densitometric Analysis
H3K27me3
H3K27ac
SFRP1
e
ACOSC4 VC
ACOSC4 Sfrp1 OE
ACOSC4+DAC
ACOSC4 Sfrp1 OE+DAC
ACOSC3 VC
ACOSC3 Sfrp1 OE
ACOSC3+DAC
ACOSC3 Sfrp1 OE+DAC
H3K27me3
H3K27ac
SFRP1
H3
β-Tubulin
17 kDa
17 kDa
35 kDa
17 kDa
55 kDa
f
ACOSC4 VC
ACOSC4 Sfrp1 OE
ACOSC4+DAC
ACOSC4 Sfrp1 OE+DAC
ACOSC3 Sfrp1 OE+DAC
ACOSC3+DAC
ACOSC3 Sfrp1 OE
ACOSC3 VC
Densitometric Analysis
H3K27me3
H3K27ac
SFRP1
g
Enrichment plot: HALLMARK_HYPOXIA
Enrichment score (ES)
Ranked list metric (Signal2Noise)
Rank in Ordered Dataset
Enrichment profile
Hits
Ranking metric scores
Hallmark Hypoxia
h
% of the Input SOX2 ChIP
p=0.0095
p=0.037
Bead Control
IgG Control
A3886 VC
A3886 Sfrp1 OE
A3886+DAC
A3886 Sfrp1 OE+DAC
HIF1α promoter
i
% of the Input SOX2 ChIP
p=0.0485
p=0.0447
Bead Control
IgG Control
ACOSC4 VC
ACOSC4+DAC
ACOSC4 Sfrp1 OE
ACOSC4 Sfrp1 OE+DAC
ACOSC3 VC
ACOSC3+DAC
ACOSC3 Sfrp1 OE
ACOSC3 Sfrp1 OE+DAC
HIF1α promoter
j
Enrichment plot: HALLMARK_GLYCOLYSIS
Enrichment score (ES)
Ranked list metric (Signal2Noise)
Rank in Ordered Dataset
Enrichment profile
Hits
Ranking metric scores
Hallmark Glycolysis
k
SLC2A2
HK2
HIF1A
LDHA
SOX2
l
A3886 VC
A3886 Sfrp1 OE
A3886+DAC
A3886 Sfrp1 OE+DAC
% of the Input HIF1α ChIP
p=0.08
p=0.001
p=0.001
Bead Control
IgG Control
SLC2A2
HK2
LDHA
m
ACOSC4 VC
ACOSC4 Sfrp1 OE
ACOSC4+DAC
ACOSC4 Sfrp1 OE+DAC
ACOSC3 Sfrp1 OE+DAC
ACOSC3+DAC
ACOSC3 Sfrp1 OE
ACOSC3 VC
% of the Input HIF1α ChIP
p=0.072
p=0.002
p=0.002
p=0.001
p=0.008
p=0.001
Bead Control
IgG Control
SLC2A2
HK2
LDHA

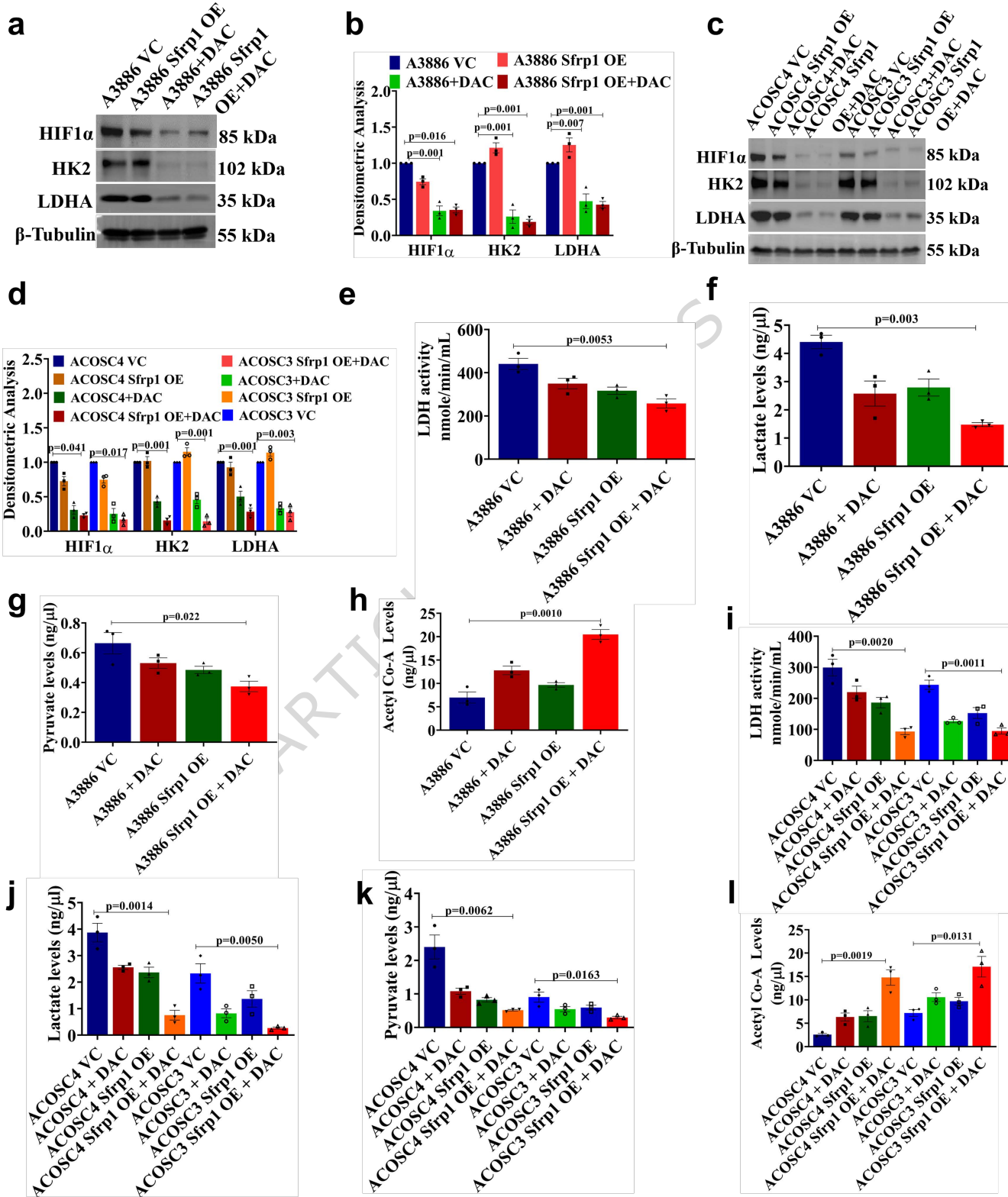
a
A3886 VC
A3886 Sfrp1 OE
A3886+DAC
A3886 Sfrp1 OE+DAC
HIF1α
HK2
LDHA
β-Tubulin
85 kDa
102 kDa
35 kDa
55 kDa
b
A3886 VC
A3886 Sfrp1 OE
A3886+DAC
A3886 Sfrp1 OE+DAC
Densitometric Analysis
HIF1α
HK2
LDHA
c
ACOSC4 VC
ACOSC4 Sfrp1 OE
ACOSC4+DAC
ACOSC4 Sfrp1 OE+DAC
ACOSC3 VC
ACOSC3 Sfrp1 OE
ACOSC3+DAC
ACOSC3 Sfrp1 OE+DAC
d
ACOSC4 VC
ACOSC4 Sfrp1 OE
ACOSC4+DAC
ACOSC4 Sfrp1 OE+DAC
ACOSC3 Sfrp1 OE+DAC
ACOSC3+DAC
ACOSC3 Sfrp1 OE
ACOSC3 VC
Densitometric Analysis
HIF1α
HK2
LDHA
e
LDH activity nmole/min/mL
p=0.0053
A3886 VC
A3886 + DAC
A3886 Sfrp1 OE
A3886 Sfrp1 OE + DAC
f
Lactate levels (ng/µl)
p=0.003
g
Pyruvate levels (ng/µl)
p=0.022
h
Acetyl Co-A Levels (ng/µl)
p=0.0010
i
LDH activity nmole/min/mL
p=0.0020
p=0.0011
j
Lactate levels (ng/µl)
p=0.0014
p=0.0050
k
Pyruvate levels (ng/µl)
p=0.0062
p=0.0163
l
Acetyl Co-A Levels (ng/µl)
p=0.0019
p=0.0131

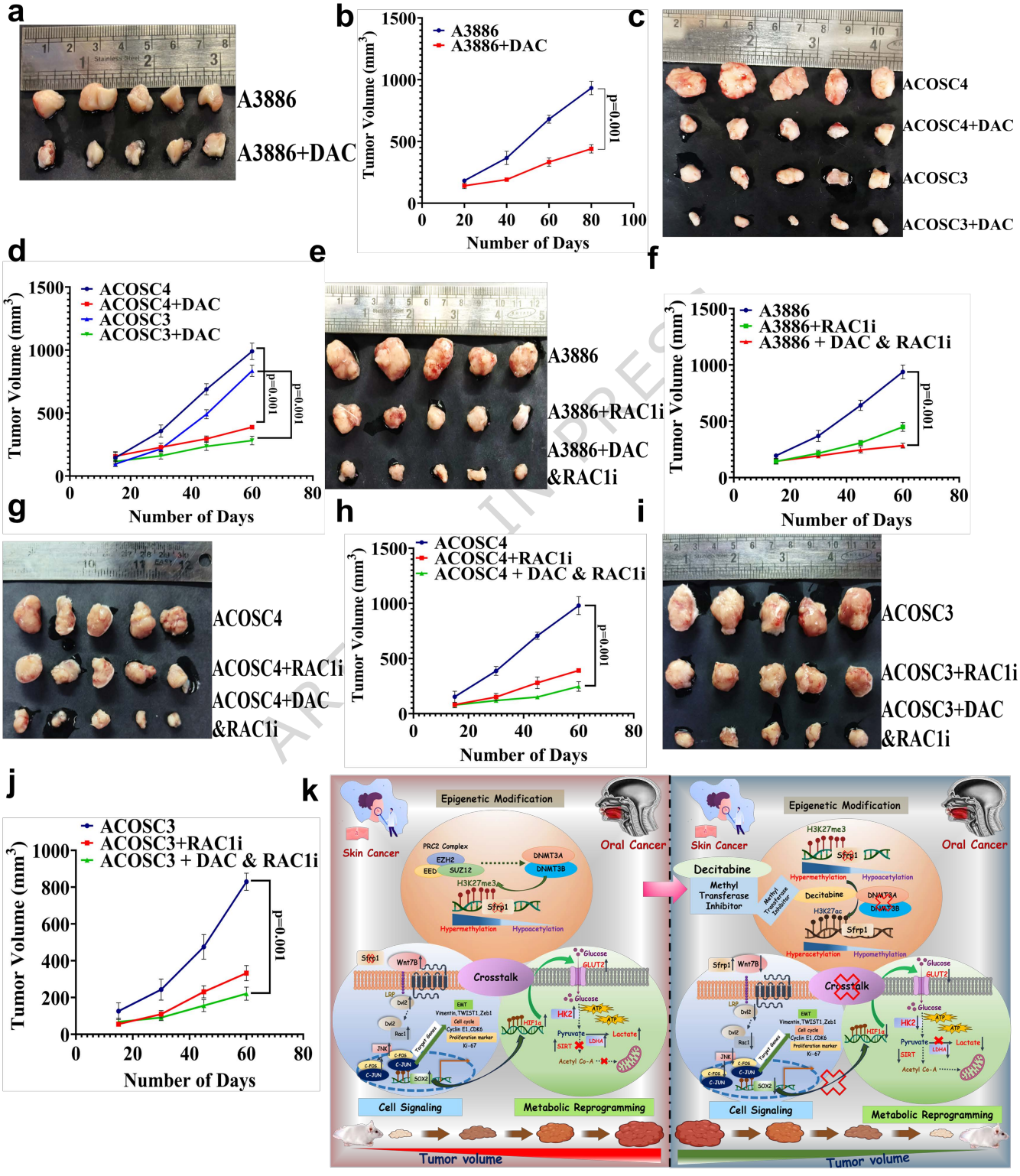
a
A3886
A3886+DAC
b
A3886
A3886+DAC
Tumor Volume (mm3)
Number of Days
p=0.001
c
ACOSC4
ACOSC4+DAC
ACOSC3
ACOSC3+DAC
d
ACOSC4
ACOSC4+DAC
ACOSC3
ACOSC3+DAC
Tumor Volume (mm3)
Number of Days
p=0.001
p=0.001
e
A3886
A3886+RAC1i
A3886+DAC &RAC1i
f
A3886
A3886+RAC1i
A3886 + DAC & RAC1i
Tumor Volume (mm3)
Number of Days
p=0.001
g
ACOSC4
ACOSC4+RAC1i
ACOSC4+DAC &RAC1i
h
ACOSC4
ACOSC4+RAC1i
ACOSC4 + DAC & RAC1i
Tumor Volume (mm3)
Number of Days
p=0.001
i
ACOSC3
ACOSC3+RAC1i
ACOSC3+DAC &RAC1i
j
ACOSC3
ACOSC3+RAC1i
ACOSC3 + DAC & RAC1i
Tumor Volume (mm3)
Number of Days
p=0.001
k
Skin Cancer
Oral Cancer
Epigenetic Modification
PRC2 Complex
EZH2
EED
SUZ12
DNMT3A
DNMT3B
H3K27me3
Sfrp1
Hypermethylation
Hypoacetylation
Crosstalk
Wnt7B
LRP
Dvl2
Rac1
JNK
C-FOS
C-JUN
SOX2
EMT
Vimentin, TWIST1, Zeb1
Cell cycle
Cyclin E1, CDK6
Proliferation marker
Ki-67
Target Genes
Glucose
GLUT2
HK2
ATP
HIF1α
Pyruvate
Lactate
SIRT
LDHA
Acetyl Co-A
SIRT6
Cell Signaling
Metabolic Reprogramming
Tumor volume
Decitabine
Methyl Transferase Inhibitor
H3K27me3
H3K27ac
Hyperacetylation
Hypomethylation